

Seasonal and Interannual Variability of the
Sargasso Sea Plankton Community

by

Amy Hansen

A Thesis Presented in Partial Fulfillment
of the Requirements for the Degree
Master of Science

Approved November 2010 by the
Graduate Supervisory Committee:

Susanne Neuer, Chair
Rosa Krajmalnik-Brown
Milton Sommerfeld

ARIZONA STATE UNIVERSITY

December 2010

ABSTRACT

Phytoplankton comprise the base of the marine food web, and, along with heterotrophic protists, they are key players in the biological pump that transports carbon from the surface to the deep ocean. In the world's subtropical oligotrophic gyres, plankton communities exhibit strong seasonality. Winter storms vent deep water into the euphotic zone, triggering a surge in primary productivity in the form of a spring phytoplankton bloom.

Although the hydrographic trends of this “boom and bust” cycle have been well studied for decades, community composition and its seasonal and annual variability remains an integral subject of research. It is hypothesized here that proportions of different phytoplankton and protistan taxa vary dramatically between seasons and years, and that picoplankton represent an important component of this community and contributor to carbon in the surface ocean. Monthly samples from the Bermuda Atlantic Time-series Study (BATS) site were analyzed by epifluorescence microscopy, which permits classification by morphology, size, and trophic type. Epifluorescence counts were supplemented with flow cytometric quantification of *Synechococcus*, *Prochlorococcus*, and autotrophic pico- and nanoeukaryotes.

Results from this study indicate *Synechococcus* and *Prochlorococcus*, prymnesiophytes, and hetero- and mixotrophic nano- and dinoflagellates were the major players in the BATS region plankton community. Ciliates, cryptophytes, diatoms, unidentified phototrophs, and other taxa represented rarer groups. Both flow cytometry and epifluorescence microscopy revealed *Synechococcus* to be

most prevalent during the spring bloom. Prymnesiophytes likewise displayed distinct seasonality, with the highest concentrations again being noted during the bloom. Heterotrophic nano- and dinoflagellates, however, were most common in fall and winter. Mixotrophic dinoflagellates, while less abundant than their heterotrophic counterparts, displayed similar seasonality.

A key finding of this study was the interannual variability revealed between the two years. While most taxa were more abundant in the first year, prymnesiophytes experienced much greater abundance in the second year bloom. Analyses of integrated carbon revealed further stark contrasts between the two years, both in terms of total carbon and the contributions of different groups. Total integrated carbon varied widely in the first study year but displayed less fluctuation after June 2009, and values were noticeably reduced in the second year.

ACKNOWLEDGMENTS

This research was supported by NSF BIO-OCE Grant 0752592 and TA/RA funding from the Arizona State University School of Life Sciences. I thank Jessica Amacher, Alexandra Freibott, and Rebecca Mestek for their assistance with microscopy identification and, in the case of Ms. Freibott, for sharing her preliminary results on ciliate taxonomy and abundance at the BATS station. Sincere thanks go to Dr. Michael Lomas of the Bermuda Institute of Ocean Sciences for providing hydrography and FCM data, and for helpful discussions on the context and relevance of this study. This research would not have been possible if not for the tireless efforts of the scientists and crew aboard the *R/V Atlantic Explorer*. Finally, I am extremely grateful to Dr. Susanne Neuer for her insights into and support of my research during my time at ASU.

TABLE OF CONTENTS

	Page
LIST OF TABLES.....	v
LIST OF FIGURES.....	vi
INTRODUCTION.....	1
METHODS.....	8
At-Sea Sampling and Processing.....	8
Flow Cytometry Sample Processing.....	10
Epifluorescence Microscope Slide Counting.....	10
Conversion of Cell Abundance to Biovolume.....	14
Conversion of Biovolume to Carbon.....	15
Calculating Integrated Chlorophyll <i>a</i> and Carbon.....	15
Contour Plots.....	17
RESULTS.....	18
Hydrographic Data.....	18
Flow Cytometry Data.....	22
Epifluorescence Microscopy Counts, Biovolume, and Carbon.....	25
DISCUSSION.....	42
REFERENCES.....	58
APPENDIX	
A ABBREVIATIONS AND ACRONYMS USED.....	62
B CRUISE DATES AND DEPTHS.....	64

LIST OF TABLES

Table	Page
1. Organisms or taxonomic groups counted in epifluorescence microscopy slide counts.....	12
2. Carbon conversion equations compiled from the literature and used in this study.....	16

LIST OF FIGURES

Figure	Page
1. Location of Bermuda and the BATS site	8
2. Contour plot of temperature.....	18
3. Contour plot of Chl <i>a</i>	19
4. Integrated Chl <i>a</i> from 0-150 m	20
5. Contour plot of primary production.....	21
6. Contour plots of nutrient concentrations	22
7. Contour plots of <i>Synechococcus</i> and <i>Prochlorococcus</i> abundance from FCM data.....	23
8. Contour plots of picoeukaryote and nanoeukaryote abundance from FCM data.....	25
9. Contour plot of <i>Synechococcus</i> abundance	26
10. Contour plot of prymnesiophyte abundance	27
11. Average prymnesiophyte abundance per month.....	29
12. Contour plots of HNF and HDF abundance and C	30
13. Total HNF and HDF abundance per month	32
14. Contour plot of MDF abundance.....	33
15. Total MDF abundance per month.....	34
16. Contour plots of total, centric, and pennate diatom abundance.....	36
17. Contour plot of cryptophyte abundance	37
18. Integrated C per month from 0-150 m.....	38

Figure		Page
19.	Percent contributions of different groups to integrated C per month.....	39
20.	Relationship of integrated Chl <i>a</i> to integrated autotrophic C	41

INTRODUCTION

The deep, clear open ocean appears empty at first glance. These blue waters are so oligotrophic, or bereft of nutrients, that oceanographers refer to them as “deserts.” With none of the hustle and bustle that characterizes coastal kelp forests or coral reefs, it is easy to fall prey to the illusion that these seas are practically lifeless. Peer at them through a microscope, however, and a different picture emerges.

Microorganisms dominate the world’s oligotrophic ocean gyres—those vast, slowly swirling bodies of water between continents set in motion by the Coriolis effect—although they are significantly less abundant here than in productive, eutrophic (nutrient-rich) zones. One such gyre is the North Atlantic Subtropical Gyre (NASTG). Also called the Sargasso Sea, the western portion of the NASTG is home to the Bermuda Atlantic Time-series Study (BATS). Decades of research at the BATS site and nearby Hydrostation “S” have led to a firm understanding of the hydrography of this region (e.g. Durand et al. 2001; Steinberg et al. 2001; Nelson et al. 2004). Winter storms bring deep, cold, nutrient-rich water to the surface. This mixing event triggers a phytoplankton bloom in the euphotic zone, the upper region of the ocean where light is sufficient to allow photosynthesis. The spring bloom (which actually lasts from late winter to early spring) sees a flush of productivity as photosynthetic microbes race to take advantage of the sudden supply of nutrients. When these nutrients become exhausted, the bloom ends. Warmer summer temperatures then stratify the surface waters, and most phytoplankton stay at the base of the euphotic zone, where the

disadvantage of low available light is offset by a greater amount of nutrients than at the surface. Productivity remains low until the advent of the next spring bloom.

This basic hydrographic framework can be upset or interrupted. Passing mesoscale eddies—swirling masses of seawater on the scale of tens to several hundreds of kilometers—and summer storms uplift or depress the thermocline and nutricline (the depth at which temperature or nutrient concentration, respectively, changes rapidly) (McGillicuddy et al. 2007). Changes in large-scale climatic patterns like the North Atlantic Oscillation (NAO) may also introduce variability into the system (Cattiaux et al. 2010; Lomas et al. 2010). Nelson and colleagues (2004) found significant climate-induced variability, both from NAO and El Niño-Southern Oscillation (ENSO) forcing, in a roughly $6 \times 10^5 \text{ km}^2$ study region with the BATS site at the center. Each of these events directly impacts the microorganisms that form the base of the marine food web.

The vast size of ocean gyres understandably imposes limits on the study of these microscopic organisms. Tracking and analysis of the entire phytoplankton community can be accomplished by measuring chlorophyll *a* (Chl *a*), either directly or by satellite (remote proxy). However, satellites may misinterpret concentrations of Chl *a* by at least a factor of five (Dierssen 2010). Chl *a* per cell can also change with depth: shaded cells growing in dark or crowded environments may photoacclimate, or produce more Chl *a* to compensate for limited light (Dubinsky and Stambler 2009). Furthermore, these measurements do not take into account phytoplankton community diversity or the contribution of small heterotrophic plankton, which lack Chl *a*.

High-performance liquid chromatography (HPLC) pigment analysis partially addresses the issue of diversity but cannot differentiate between species or different size cells of the same species or taxa (Liu et al. 2009) and can only be applied to photosynthetic organisms. Novel molecular techniques like quantitative PCR, denaturing gradient gel electrophoresis (DGGE), and 18S rDNA clone libraries have more recently been employed (e.g. Not et al. 2007, 2008; Amacher et al. 2009) to gain a more precise taxonomic picture of plankton communities. These methods are especially useful for recognizing morphologically indistinct picoplankton whose identity eludes the traditional microscopist (Not et al. 2008). Flow cytometry (FCM) is another commonly used technique to determine abundances and, by proxy, carbon (C) contributions of different phytoplankton groups. FCM allows high-throughput sampling but may be prone to subsampling error because extremely small sample sizes are processed (Lomas et al. 2009b). Also, because FCM relies on cell size and pigmentation for cell identification, it is limited in its ability to make fine distinctions between taxa.

Durand et al. (2001) used FCM to chart seasonal phytoplankton trends at BATS. These authors found that the cyanobacteria *Prochlorococcus* and *Synechococcus* were temporally offset, with the prior at maximum abundance during late summer and fall, and the latter peaking during the spring bloom. Furthermore, eukaryotic phytoplankton abundance and contribution to C was highest during the bloom, though cell size tended to be smallest at that time.

Recently, Lomas et al. (2009b) combined HPLC pigment analysis with FCM and hydrographic analyses to characterize the phytoplankton community in

the BATS region with specific regard to species' responses to late winter (late February to early March) storms. The cyanobacteria *Prochlorococcus* and *Synechococcus* were quantified by FCM, and FCM data on eukaryotic phytoplankton was supplemented with HPLC results to quantify the abundance of pelagophytes, haptophytes, and diatoms. Only these three taxa were charted because other groups lacked signature pigments (that is, multiple groups of interest shared a pigment) or were below the level of detection. These authors reported that phytoplankton communities, and especially diatoms, respond rapidly (on the scale of days) to changing hydrographic conditions like those induced by storm events. These results, however, do not clarify the role of heterotrophic protists in the community, nor do they specifically address the detailed composition of the eukaryotic phytoplankton.

Epifluorescence microscopy is a useful tool for addressing those concerns. Samples can be fixed, frozen, and then observed months or even several years after collection. Like traditional microscopy, cells observed and counted under epifluorescence can be identified by morphology and can be sorted into size classes. Perhaps most importantly, this form of microscopy allows the scientist to distinguish between trophic types, a distinction that is often out of reach in brightfield microscopy when it comes to classifying the picoplankton component of the plankton community (Booth 1987). The plankton community is defined here as organisms smaller than 100 μm (and predominantly $<20 \mu\text{m}$) and includes the cyanobacteria (especially *Synechococcus* and *Prochlorococcus*), eukaryotic phytoplankton, and heterotrophic protists.

Caron et al. (1995) took advantage of the taxonomic precision afforded by epifluorescence microscopy, in conjunction with hydrographic data on water column structure and particulate carbon and nitrogen concentrations, to characterize the plankton community (in their study, microbes $\leq 200 \mu\text{m}$) in August 1989 and March-April 1990. They quantified heterotrophic bacteria, cyanobacteria, photo- and heterotrophic nanoplankton (2-20 μm), and hetero- and phototrophic microplankton (5-200 μm), finding that abundance of these organisms decreased in the order listed above. In both time periods studied, heterotrophic bacteria were present on the order of $10^5 \text{ cells mL}^{-1}$, cyanobacteria on the order of $10^3 \text{ cells mL}^{-1}$, nanoplankton on the order of $10^2 \text{ cells mL}^{-1}$, and microplankton ranging from <1 to $\sim 25 \text{ cells mL}^{-1}$.

Lessard and Murrell (1996) used epifluorescence microscopy to further investigate heterotroph dynamics (heterotrophic protists $>5 \mu\text{m}$, predominantly dinoflagellates and ciliates) at the BATS station with samples taken on the same cruises as Caron et al. (1995). While filtration of glutaraldehyde-fixed seawater samples is acceptable for quantification and identification of dinoflagellates, ciliates were less abundant (5-10 times less, in Lessard and Murrell's study) and were often distorted or destroyed by glutaraldehyde and filtration. Therefore, these authors also analyzed gravity-settled, Lugol's iodine-fixed samples on an inverted microscope to obtain accurate counts of ciliates. They found that heterotrophic flagellates $>5 \mu\text{m}$ were predominantly dinoflagellates (HDF), and a vast majority ($>92\%$) of HDF were $<20 \mu\text{m}$. Furthermore, flagellates $<5 \mu\text{m}$ (presumably nanoflagellates, or HNF), were "the single most important group of

protist herbivores,” accounting for ~90% of grazing in the months studied (p. 1061).

Other types of microscopy also yield information on the plankton community. Haidar and Thierstein (2001) employed light microscopy to investigate the composition and variability of the coccolithophorid community at Hydrostation “S,” near the BATS site. *Emiliana huxleyi*, the intricate, armor-plated orb that is the darling of biological oceanographers, is included in this group, which is itself part of the diverse phylum Haptophyceae or Prymnesiophyceae (Heimdal 1997). Haidar and Thierstein (2001) found that coccolithophores exhibited bloom seasonality; that is, concentrations were highest from late winter to spring and lowest in summer, a pattern thought to be followed by many phytoplankton in the Sargasso Sea.

Phytoplankton may be best known for their contribution to global primary production—they are responsible for around 50% of the world’s primary and oxygen production annually—and, along with heterotrophic protists, their fundamental role in marine food webs. However, they are equally crucial in the microbial loop, which recycles C and nutrients within the upper water column, and in the biological C pump, or the system by which C in the surface ocean is exported to the deep. There exists a growing realization that picoplankton are important players in these processes (Richardson and Jackson 2007; Amacher et al. 2009). To better understand which organisms are key players in the microbial loop and which are most likely to sink (and thus sequester C that could otherwise be respired and released in the form of greenhouse gases), it is first necessary to

gain a more complete, seasonally resolved recognition of the organisms that comprise the plankton community in the upper water column.

Knowing the composition of the plankton community is also important for microbial ecology, as the scientist must have a strong understanding of community makeup before he or she can hypothesize relationships between different players. The traditional “bottom-up,” or nutrient-driven, paradigm of biological oceanography is insufficient for understanding marine biogeochemical cycles or community interactions (Strom 2008). Developing a quantitative picture of the plankton community is important not only for gaining knowledge of cell-cell interactions and trophic cascades, but also for increasing our understanding of the biological C pump and predicting how current and future climate changes could impact ocean biology.

Although researchers have investigated particular taxonomic groups at the BATS site over extended periods of time or the extended community for short periods, such as during the spring bloom, this study took a novel approach in characterizing the seasonality of the BATS plankton community throughout the upper water column at monthly intervals for two years. By employing both epifluorescence and FCM technologies, a greater degree of precision in estimating abundances and C and in recognizing taxonomic differences in the plankton community was achieved. Understanding the range of seasonal and annual variability at the BATS site is vital for extrapolating findings beyond the study period and throughout the region.

METHODS

At-sea sampling and processing—Water column samples were collected aboard the *R/V Atlantic Explorer* at the BATS site (31°40'N, 64°10'W), located approximately 82 km SE of Bermuda in the northwestern Sargasso Sea (Fig. 1). Sampling was conducted monthly from May 2008 to April 2010, with supplementary biweekly bloom cruises during the spring bloom of each year. This time period has been split into two years: Year 1 (May 2008-April 2009) and Year 2 (May 2009-April 2010). A Sea-Bird conductivity-temperature-depth (CTD) instrument, mounted on a rosette of 24 12 L Niskin bottles and equipped with an in vivo fluorescence sensor, was used to create profiles of temperature, salinity, and fluorescence, and to collect seawater at specific depths. CTD readings were collected on the downcast (that is, as the rosette descended), and samples were collected on the upcast (that is, as the rosette ascended).

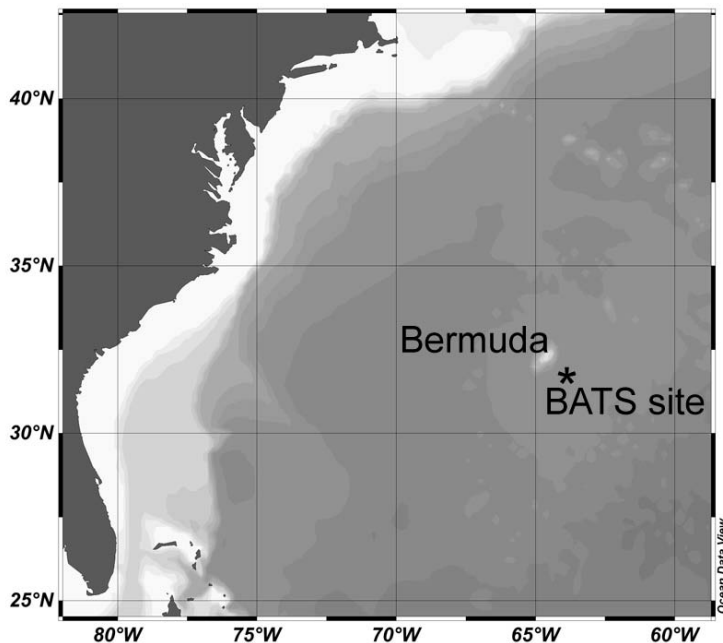


Fig. 1. Location of Bermuda (the white island underneath the letter “a”) and the BATS site (indicated by *) in the subtropical North Atlantic Ocean.

Samples for chlorophyll *a* (Chl *a*) and primary production were taken at 1, 10, 20 m, and every 20 m thereafter to 140 m. Samples for nutrient analysis (concentrations of NO_3+NO_2 (nitrate+nitrite, hereafter nitrate), NO_2 (nitrite), PO_4 (phosphate), and $\text{Si}(\text{OH})_4$ (silicate) ($\mu\text{mol kg}^{-1}$)) were taken at the same depths as Chl *a* and primary production in addition to 160 and 200 m. These data are grouped here as hydrographic data. Chl *a*, primary production, and nutrients were measured at sea or at the Bermuda Institute of Ocean Sciences (BIOS), as appropriate, as in Lomas et al. (2009a). Briefly, Chl *a* was measured at by Turner fluorometer following acetone extraction. Primary production was measured by in situ incubation and by liquid scintillation analysis. Nutrients were gravity-filtered on ship before being measured on a long-pass capillary spectrometer (at sea) or an Alpkem Flow Solution IV system (at the BIOS station).

Monthly samples for microscopy were collected in Niskin bottles at four depths chosen from the fluorescence profile created as the rosette descended. A sample was always collected at 10 m and at the deep chlorophyll maximum (DCM). The remaining two samples were collected between 10 m and the DCM (or, occasionally, one was collected below the DCM) (see Appendix B). Samples for epifluorescence microscopy slides (hereafter referred to as “slides”) were drawn, prefiltered through 100 μm nitex mesh, from the corresponding Niskins into carboys rinsed three times with seawater. A 15 and 50 mL sample was filtered for each depth. Glutaraldehyde (50 and 200 μL , respectively) was added to the 15 and 50 mL samples and inverted to mix. Just prior to filtration, 4',6-diamidino-2-phenylindole (DAPI) (200 μL or 1 mL, respectively) was added to

the 15 and 50 mL samples and inverted to mix. Samples were then filtered onto 0.2 μm black polycarbonate filters placed atop 0.45 μm nitrocellulose filters on glass filter bases with a vacuum pump run at the lower setting to avoid cell lysis. Filters were mounted in immersion oil on glass slides under glass coverslips and stored in the dark at -20°C until they could be shipped to Arizona State University (ASU) for counting.

FCM samples were taken at 1, 10, 20 m, and every 20 m thereafter down to 140 m. For processing of these samples, 1.5 mL seawater was added to labeled cryovials that had been rinsed with seawater from the corresponding Niskin. 75 μL paraformaldehyde (PFA) was added to each vial and the tubes were inverted to mix. Samples were stored at 4°C for 2 h in the dark before being transferred to liquid nitrogen, where they were kept until processing.

Flow cytometry sample processing—FCM samples were analyzed at the BIOS station as in Lomas and Moran (2010). Briefly, a Becton Dickinson Influx cytometer equipped with a 488 nm blue excitation laser and Chl *a* and phycoerythrin bandpass filters was used to quantify *Synechococcus*, *Prochlorococcus*, and autotrophic picoeukaryotes ($\sim 1\text{-}3\ \mu\text{m}$) and nanoeukaryotes ($>3\ \mu\text{m}$).

Epifluorescence microscope slide counting—Slide-mounted filters were analyzed with the 100X objective under oil immersion on a Zeiss Axio Imager.A1 epifluorescence microscope. Both blue light (Zeiss filter set 09 with 450-490 nm excitation) and UV light (Zeiss filter set 34 with 390 nm excitation) were used. Organisms were categorized into the taxonomic, morphological, and functional

groups listed in Table 1 based on cell morphology, size, pigmentation under blue-light excitation, and nuclear structure and relative brightness of the DAPI-stained nucleus or nuclei under UV-light excitation. To elaborate, prymnesiophytes were identified by their wing-like red chloroplasts on either side of a tall, thin, central green nucleus; this morphology was clear even for cells in the smallest size class.

For the heterotrophic flagellates, which appear green under blue light (Lessard and Murrell 1996), heterotrophic nanoflagellates (HNF) refers to cells in the 1-2 and 2-5 μm size classes, and heterotrophic dinoflagellates (HDF) refers to cells in the larger size classes; for these organisms and others grouped into size classes, the largest measured dimension determined in which class the cell was placed. These size classes were based on the existing literature: Lessard and Murrell (1996) showed that HDF in this region were mainly $<20 \mu\text{m}$, and other studies cited by these authors found that most heterotrophic flagellates were generally $<5 \mu\text{m}$. The present study split the 1-5 and 5-20 μm ranges into more precise size classes to better define this component of the plankton community. Flagellae were not visible on all HNF and HDF cells.

Mixotrophic dinoflagellates (MDF) were identified based on their green body color, red chloroplast(s), and bright dinokaryon. No 1-2 μm MDF were counted because such small cells would have been indistinguishable from 1-2 μm prymnesiophytes. On rare occasions, an MDF's red chloroplast, when viewed under UV excitation, was revealed to be a recently engulfed phototrophic organism. In these cases, the cell was classified as an HDF of the appropriate size class (Lessard and Swift 1986). The cyanobacterium *Prochlorococcus* could not

Table 1. Organisms or taxonomic groups counted in epifluorescence microscopy slide counts. Groups indicated by an asterisk (*) were counted in every slide. Other groups were counted if they were presented in a stripe across the filter. Other organisms not listed here were assigned names based on their particular morphology, pigmentation, and size. BV: biovolume. DAPI: 4',6-diamidino-2-phenylindole. UV: ultraviolet light.

Organism or taxonomic group	Size or size class (μm)	Typical shape	Applied BV shape	Pigmentation under blue light	DAPI stain appearance under UV, if noteworthy
<i>Synechococcus</i> *	1	Circular	Sphere	Yellow	
Prymnesiophytes*	1-2, 2-4, 4-6, >6	Circular	Sphere	Dual red chloroplasts, central green nucleus	
Heterotrophic Nano- and Dinoflagellates*	1-2, 2-5, 5-10, 10-15, 15-20, >20	Circular or prolate	Prolate sphere	Green	Bright dinokaryon
Mixotrophic Dinoflagellates*	2-5, 5-10, 10-15, 15-20, >20	Prolate	Prolate sphere	Green with red chloroplast(s)	Bright dinokaryon
Autotrophic Dinoflagellates	Varied	Prolate	Prolate sphere	Red	Bright dinokaryon
Ciliates	Varied	Circular or prolate, fringed by cilia	Sphere or prolate sphere	Green, occasionally some red	Multiple bright nuclei
Cryptophytes	Generally 2-8	Oval with pointed end	Sphere or prolate sphere	Orange, green edge	
Diatoms: Centric	Varied	Circular or rectangular	Cylinder	Green frustule and nucleus, red chloroplasts	
Diatoms: Pennate	Varied	Long and thin with tapered ends	Parallelepiped (rectangular box)	Green frustule and nucleus, red chloroplasts	
Phototrophs	Generally 2-10	Circular or prolate	Sphere or prolate sphere	Red	

be quantified from slide counts because the black filter background masks its dark red pigmentation under blue light.

Dominant taxa—those that appeared in relatively high densities (≥ 30 cells in 10 fields) (Neuer and Cowles 1994) in a given sample—were counted in 5 or 10 fields distributed evenly across the entire filter. Less abundant organisms were counted in a stripe extending the diameter of the filter. The 50 mL filter was counted in all save three cases where that filter was damaged, missing, or too crowded to count accurately (see Appendix B). In two of the three cases, the 15 mL filter sported very few cells relative to the number of cells seen in adjacent depths for that month, and two stripes were counted on the 15 mL filter to compensate for this scarcity. Cell counts were converted to cells mL⁻¹ by means of field-specific conversion factors incorporating the filtration volume, number of cells counted, and size of the field counted (the “large square” on the microscope ocular, field of view, or stripe).

Subsampling error is inherent in the data collected in this study (Venrick 1978). That is, the data were extrapolated from the counted portion of a 50 mL filtered sample collected at one depth at one point in time from a single location in the sea. This approach is unavoidably necessary, given the expense of conducting marine research cruises, the vast size of the NASTG, and the fact that microscopy is a very time-consuming enterprise. Nonetheless, the results presented here must be considered in the context of this intrinsic error.

Confidence intervals (CI) (95%) for cell abundance from slide counts were calculated based on a Poisson distribution from the equations given in Lund et al.

(1958), assuming random distribution of organisms on the filter. In cases where the given abundance in a particular sample was a sum of multiple size classes (e.g. prymnesiophytes, which were often counted in different fields depending on the abundance of each class), the upper and lower 95% confidence limits were first calculated for each size class. These values were then summed to determine the 95% CI for that group. In the text, 95% CI are presented in parentheses after determined cell abundance.

Conversion of cell abundance to biovolume—Cell abundances (cells mL⁻¹) were converted to biovolume (BV) (μm³ mL⁻¹) using the geometric equations in Hillebrand et al. (1999) (see Table 1). Previous authors (Verity et al. 1992; Menden-Deuer and Lessard 2000; Sohrin et al. 2010) found that cells with complex morphology, such as thecate dinoflagellates, can be classified as spheres, prolate spheres, or other simple shapes with little effect on calculated BV. For non-spherical cells, the third or “hidden” dimension, which cannot be measured by traditional epifluorescence microscopy, was assumed to be equal to the smaller of the two measured dimensions.

The BV of organisms counted in size classes (prymnesiophytes, HNF, HDF, and MDF; see Table 1) were calculated from averaged cell sizes. For prymnesiophytes, cells were assumed to be 1, 3, 5, and 7 μm in diameter, respectively. For HNF, HDF, and MDF, 10 cells of the largest two size classes, which are less abundant, and 20 cells of the other size classes were measured on a representative slide (Sohrin et al. 2010), and an average length and width for each size class was calculated from these measurements.

Conversion of biovolume to carbon—C conversions from the literature are shown in Table 2. BV or logBV was applied to calculate C for each organism or taxonomic group in each sample. Initially, all conversions were applied to all cell count data, but this resulted in an extremely wide range of conversion values, stemming from the different publications' varying methodologies and chosen study organisms. This was especially problematic for calculating total C in a given sample. Therefore, one set of equations was ultimately chosen for calculating C. The three equations given by Menden-Deuer and Lessard (2000)—one for determining diatom C, one for dinoflagellates, and one for other non-diatom protists—were selected as conversion factors for this study. This was the most recent paper, and it took into account findings and limitations of previous authors. These researchers provided a unique equation for calculating dinoflagellate C—useful here because dinoflagellates were such an important taxon in the present study—as well as equations for diatom and non-diatom protists that could be efficiently applied to diverse communities like those revealed through epifluorescence microscopy.

Calculating integrated chlorophyll a and carbon—Total water column Chl *a* or C from 0-150 m, or integrated Chl *a* or C, respectively, was calculated for each month or cruise. Integrated Chl *a* ($\text{mg Chl } a \text{ m}^{-2}$) was calculated from hydrographic data, and integrated C was calculated from slide count data. To compute integrated Chl *a*, Chl *a* at a given depth ($\text{mg Chl } a \text{ m}^{-3}$) was multiplied by the depth interval (m) (i.e. the given depth minus the depth above it). These

values were then summed to determine a single value for integrated Chl *a* for that month.

Table 2. Carbon conversion equations compiled from the literature and used in this study. BV: biovolume ($\mu\text{m}^3 \text{mL}^{-1}$).

Source	Carbon conversion	
	equation ($\text{pg C } \mu\text{m}^{-3}$)	Specifications
Borsheim and Bratbak 1987	$0.22 \cdot \text{BV}$	<i>Monas</i> -like, fixed (2.5% glutaraldehyde)
Menden-Deuer and Lessard 2000	$0.760 \cdot \text{BV}^{0.819}$	Dinoflagellates
Menden-Deuer and Lessard 2000	$0.288 \cdot \text{BV}^{0.811}$	Diatoms
Menden-Deuer and Lessard 2000	$0.216 \cdot \text{BV}^{0.939}$	Non-diatom protists
Mullin et al. 1966	$10^{[(0.76 \cdot \log \text{BV}) - 0.29]}$	None (for all plankton)
Putt and Stoecker 1999	$0.19 \cdot \text{BV}$	Oligotrichous ciliates, fixed (2% Lugol's)
Strathmann 1967	$10^{[-0.314 + (0.712 \cdot \log \text{BV})]}$	Diatoms
Verity et al. 1992	$0.36 \cdot \text{BV}$	Cell BV $10^1 \mu\text{m}^3$
Verity et al. 1992	$0.24 \cdot \text{BV}$	Cell BV $10^2 \mu\text{m}^3$
Verity et al. 1992	$0.16 \cdot \text{BV}$	Cell BV $10^3 \mu\text{m}^3$
Verity et al. 1992	$0.47 \cdot \text{BV}$	<i>Synechococcus</i>

Integrated C was calculated in a similar fashion: total pg C cm^{-3} in a given sample, computed from the appropriate equations given by Menden-Deuer and Lessard (2000) (see Table 2), was multiplied by the depth interval times $1 \times 10^6 \text{cm}^3 \text{m}^{-3}$ (to convert pg C cm^{-3} into pg C m^{-3}), and these four values were summed

to determine that month's integrated C. Integrated C was also calculated for each major group (see Table 1) to determine relative monthly contributions of each group to total integrated C; rarer organisms were grouped into a single category in this instance. Values of integrated C were then converted to mg C m^{-2} .

Contour plots—Ocean Data View (ODV) software was used to create contour plots of hydrographic data, FCM cell abundance, and slide-derived cell abundance, BV, or C throughout the upper water column (0-150 m) over the course of the study period. For each, a gridded field (VG gridding) was created with depth plotted on the y-axis and time (roughly May 2008-April 2010) plotted on the x-axis. The z-axis variable and scale depended on the variable being plotted (e.g. temperature or prymnesiophyte abundance).

RESULTS

Hydrographic data—Thermal stratification (summer and fall) and deep mixing (winter and spring) are apparent in Fig. 2 in both Year 1 (May 2008-April 2009) and Year 2 (May 2009-April 2010). Stratification lasted for a longer period of time and led to a deeper mixed layer depth (MLD) in Year 2 than Year 1. Foul weather prevented cruises in January of both years, so the beginning of deep winter mixing has been extrapolated in both cases between December and February.

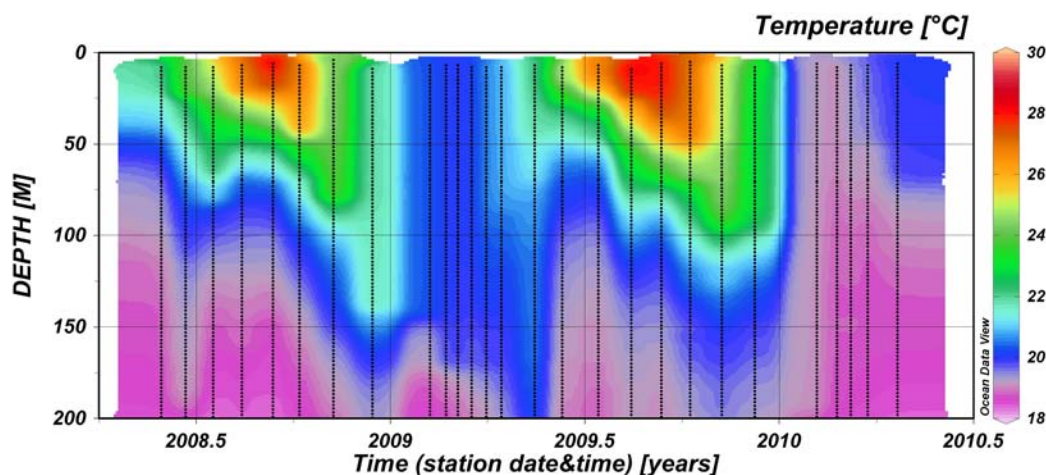


Fig. 2. Contour plot of temperature (°C) from monthly and, during bloom periods, biweekly CTD casts at the BATS site from May 2008 to April 2009. Black dots indicate sampling points. In the time scale (x-axis), 2008.5 indicates the middle of 2008 (30 June 2008), 2009 indicates 1 January 2009, and so on.

Concentrations of Chl *a* (Fig. 3) were highest during the Year 2 bloom (late winter/early spring 2010) (maximum of 0.84 mg m⁻³, early April 2010, 60

m), followed by the Year 1 bloom (maximum of 0.66 mg m^{-3} , late February 2009, 120 m). Concentrations were lowest from mid to late 2009. Data are not available for October or December 2008, September or October 2009, or January of both years, so values have been extrapolated in each case between available months, and the beginnings of both the Year 1 and Year 2 blooms have been estimated. The DCM generally occurred between 100 and 140 m throughout the study period except in the spring bloom of 2010, when it rose to $\sim 60 \text{ m}$ (early April 2010). Integrated Chl *a* (Fig. 4) remained relatively steady through Year 1 (mean: $26.55 \text{ mg Chl } a \text{ m}^{-2}$), peaking at $39.22 \text{ mg Chl } a \text{ m}^{-2}$. By contrast, values in Year 2 dropped sharply in fall 2009 before rising to a sharp peak at $83.87 \text{ mg Chl } a \text{ m}^{-2}$ in early April 2010 near the end of the spring bloom.

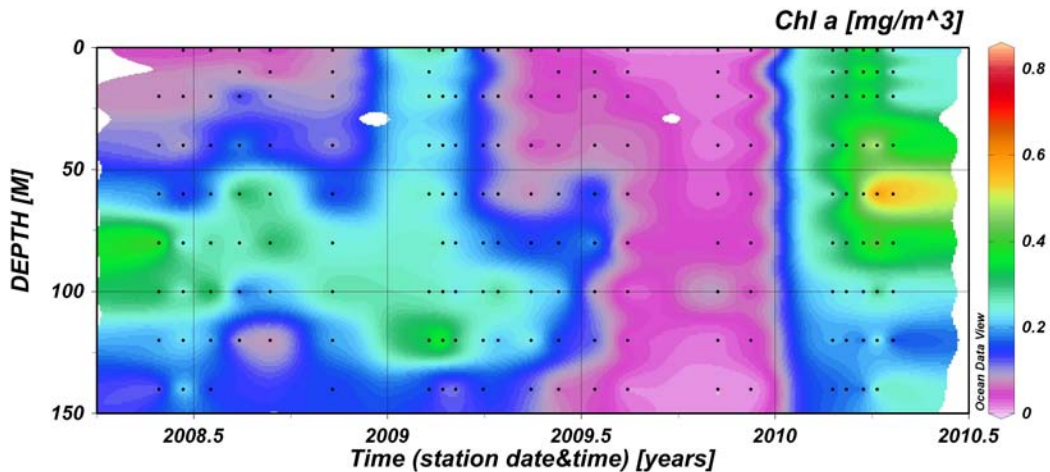


Fig. 3. Contour plot of Chl *a* (mg m^{-3}) from monthly and, during bloom periods, biweekly sampling at the BATS site from May 2008 to April 2010. Black dots indicate sampling points. In the time scale (x-axis), 2008.5 indicates the middle of 2008 (30 June 2008), 2009 indicates 1 January 2009, and so on.

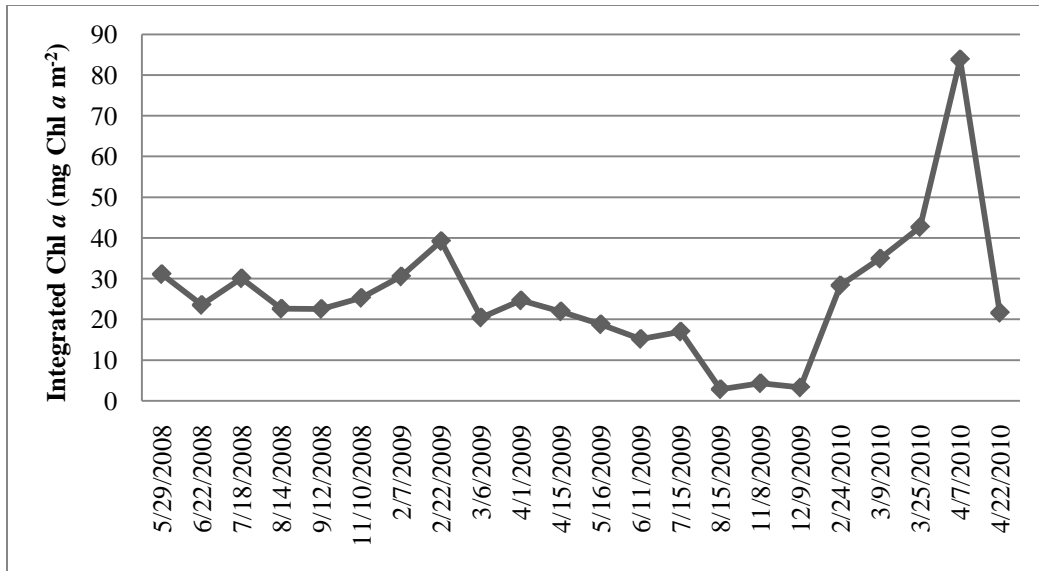


Fig. 4. Integrated Chl *a* (mg Chl *a* m⁻²) from 0-150 m. Data are from monthly and, during bloom periods, biweekly sampling at the BATS site from May 2008 to April 2010.

Primary production, an indicator of organic matter production by phytoplankton, was highest in February 2009 (15.79 mg C m⁻³ d⁻¹, early February, 20 m, and 16.40 mg C m⁻³ d⁻¹, late February, 1 m) (Fig. 5). An isolated peak also occurred in July 2009 at 60 m (15.83 mg C m⁻³ d⁻¹). Primary production was minimal below ~100 m throughout the sampling period. Mean primary production from 0-140 m was not significantly different (Student's t-test, $p=0.542$) between the two years (3.21 and 2.97 mg C m⁻³ d⁻¹ for Year 1 and Year 2, respectively). Integrated primary production (0-150 m) ranged from 189.67 to 847.27 mg C m⁻² d⁻¹ (early April 2009 and early February 2009, respectively), with three peaks (early February 2009, July 2009, late February 2010) (data not shown) that corresponded to the points of high production in Fig. 5. Maximum integrated

production was greater in winter 2009 ($847.27 \text{ mg C m}^{-2} \text{ d}^{-1}$, early February 2009) than in winter 2010 ($658.98 \text{ mg C m}^{-2} \text{ d}^{-1}$, late February 2010).

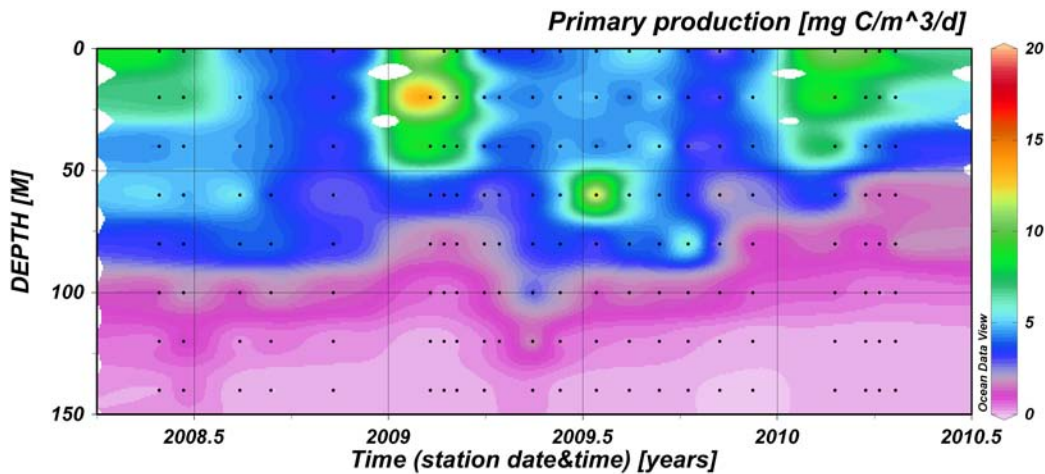


Fig. 5. Contour plot of primary production ($\text{mg C m}^{-3} \text{ d}^{-1}$) from monthly and, during bloom periods, biweekly sampling at the BATS site from May 2008 to April 2010. Black dots indicate sampling points. In the time scale (x-axis), 2008.5 indicates the middle of 2008 (30 June 2008), 2009 indicates 1 January 2009, and so on.

Fig. 6 displays nutrient concentrations from 0-200 m at the BATS site. Nutrient data are only available through March 2009, and no data are available for January 2009. With the exception of an increase in silicate in December 2008, no increases in nutrients throughout the water column relative to pre-bloom values were seen in winter, although nitrite levels were relatively high in the last available month, March 2009. Nitrate was minimal above 100 m for all months, and concentrations were highest at depth, with the highest concentrations occurring in February and March 2009 at 200 m. Nitrite was very low (<0.05

$\mu\text{mol kg}^{-1}$) throughout except for peak at 80 m in May 2008 and values up to 0.21 $\mu\text{mol kg}^{-1}$, increasing with depth, in March 2009. Concentrations of phosphate were minimal above 100 m and, like nitrate, increased with depth; however, this nutrient peaked in October 2008 at 0.14 $\mu\text{mol kg}^{-1}$, with slightly lesser peaks in July 2008 and March 2009. Silicate concentrations were highest in July 2008 from ~120-200 m and at 200 m from October 2008 to March 2009.

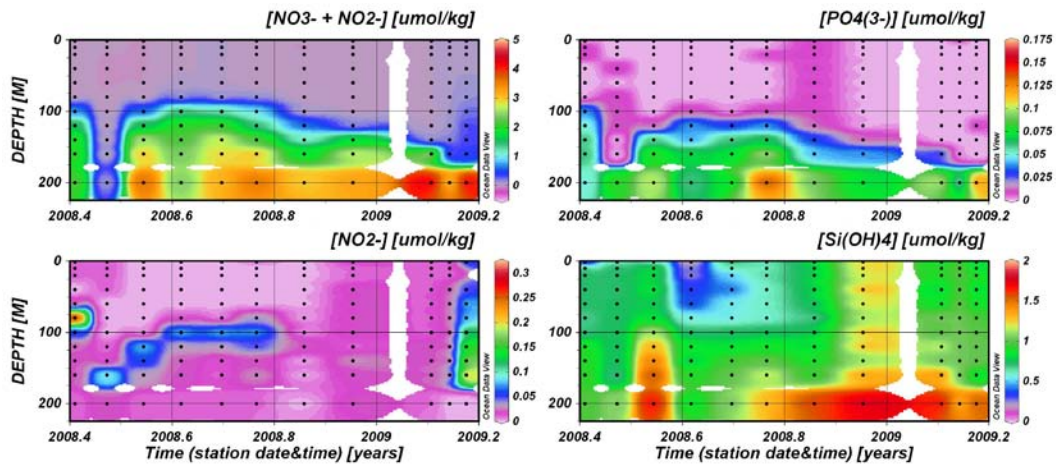


Fig. 6. Contour plot of nutrient concentrations ($\mu\text{mol kg}^{-1}$) from monthly and, during bloom periods, biweekly sampling at the BATS site from May 2008 to March 2009. Nitrate, top left; nitrite, bottom left; phosphate, top right; and silicate, bottom right. Black dots indicate sampling points. In the time scale (x-axis), 2008.4 indicates May 2008, 2008.6 indicates August 2008, 2008.8 indicates November 2008, etc.

Flow cytometry data—Concentrations of *Synechococcus* from FCM measurements ranged from 0 to 4.2×10^4 cells mL^{-1} (September 2008, 140 m, and May 2008, 40 m, respectively). *Prochlorococcus* abundances were higher overall,

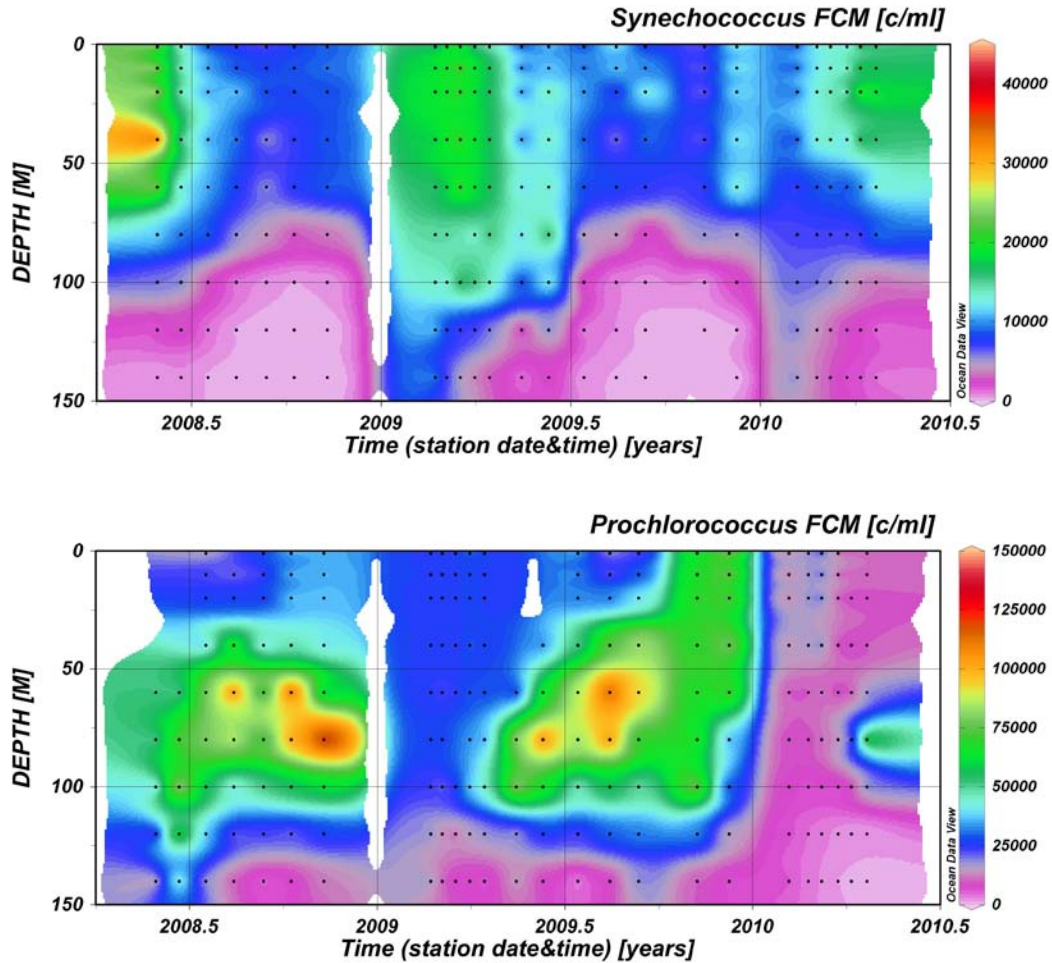


Fig. 7. Contour plots of *Synechococcus* (top) and *Prochlorococcus* (bottom) abundance (cells mL⁻¹) from monthly and, during bloom periods, biweekly sampling at the BATS site from May 2008 to April 2010, as determined by FCM. Black dots indicate sampling points. In the time scale (x-axis), 2008.5 indicates the middle of 2008 (30 June 2008), 2009 indicates 1 January 2009, and so on.

ranging from 450 to 1.4×10^5 cells mL⁻¹ (early April 2010, 140 m and October 2008, 60 m, respectively). These data reveal a temporal and spatial offset between

these two key cyanobacteria (Fig. 7), as seen in Durand et al. (2001).

Synechococcus was most prevalent in the spring blooms and decreased in abundance from surface to depth, while *Prochlorococcus* abundance peaked from early summer to late fall between 50-100 m.

The abundance of picoeukaryotes ($\sim 1-3 \mu\text{m}$) determined by FCM (Fig. 8) remained low (approximately $100-2000 \text{ cells mL}^{-1}$) relative to cyanobacteria both spatially and temporally until the beginning of 2010. There were two isolated peaks in concentration of these cells, one occurring in May 2008 at 80 m ($9181 \text{ cells mL}^{-1}$), and the other in July 2009 at 60 m ($5376 \text{ cells mL}^{-1}$). Data are not available from December 2008 to early February 2009. Mean abundance of picoeukaryotes increased slightly from 1109 to 2001 cells mL^{-1} between November 2008 and late February 2009. This difference between late winter and bloom concentrations was much more pronounced in Year 2, in which December 2009 averaged 313 cells mL^{-1} and early February 2010 had a mean of 3610 cells mL^{-1} .

Nano-eukaryote ($>3 \mu\text{m}$) abundance was notably lower than that of picoeukaryotes (Fig. 8). These cells tended to be found above 100 m. Abundance during Year 2 was lower than in Year 1, and most cells during this time occurred above approximately 75 m. Data are unavailable from November 2008 through April 2009 for most depths.

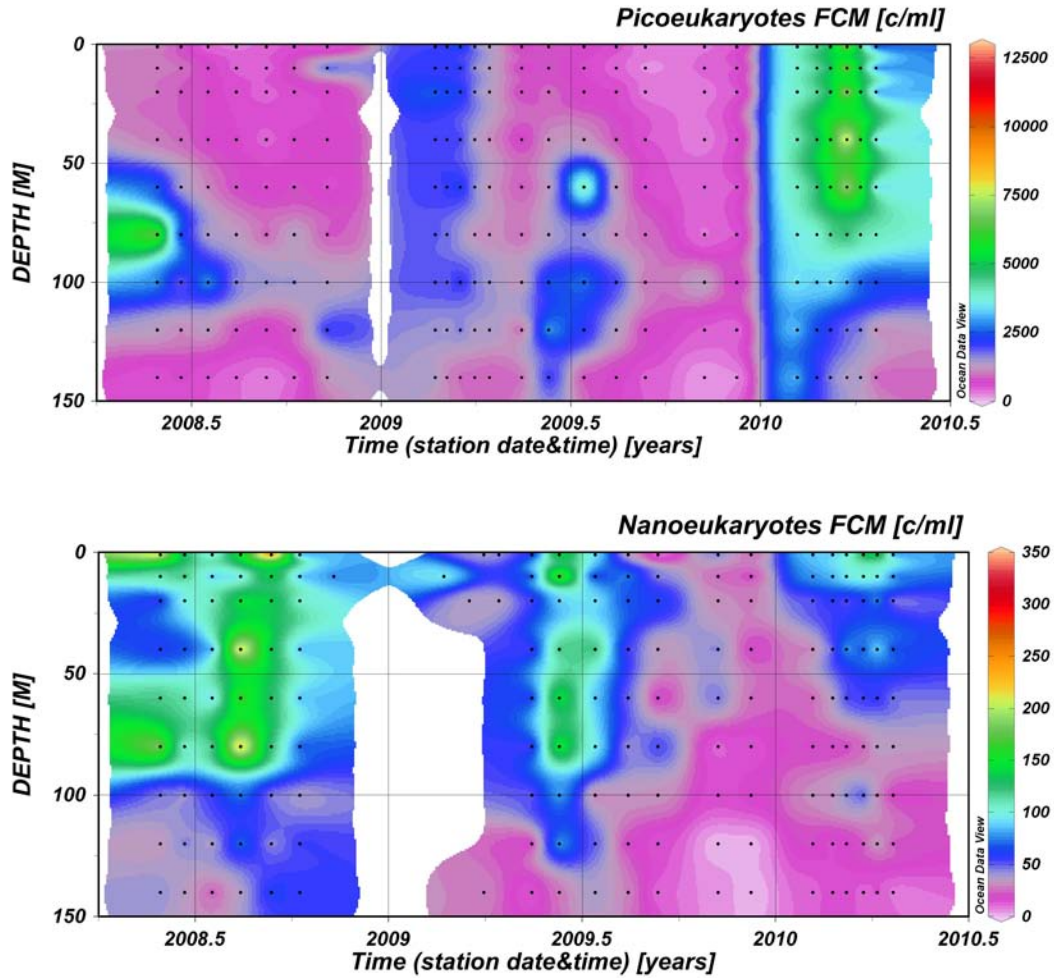


Fig. 8. Contour plots of picoeukaryote (top) and nanoeukaryote (bottom) abundance (cells mL⁻¹) from monthly and, during bloom periods, biweekly sampling at the BATS site from May 2008 to April 2010, as determined by FCM. Black dots indicate sampling points. In the time scale (x-axis), 2008.5 indicates the middle of 2008 (30 June 2008), 2009 indicates 1 January 2009, and so on.

*Epifluorescence microscopy counts, biovolume, and carbon—
 Synechococcus* ranged from 17 to 1.21x10⁵ (CI: 8-36 to 1.09-1.34x10⁵,

respectively) cells mL⁻¹, with low concentrations predominantly occurring at depth (below 100 m). Abundance (Fig. 9) was greater in the Year 1 bloom (approximately January-April 2009) than in that of Year 2. *Synechococcus* tended to be more prevalent (and therefore contributed more to overall BV and C) above approximately 80 m. May 2008 showed *Synechococcus* at concentrations approaching bloom concentrations, but this was not seen in May 2009. Slides for March 2009 were recounted to check the existence of two isolated peaks at 25 and 90 m (both ~1.20x10⁵ (CI: 1.08-1.34x10⁵) cells mL⁻¹), but the relative paucity of cells at 10 and 60 m was confirmed.

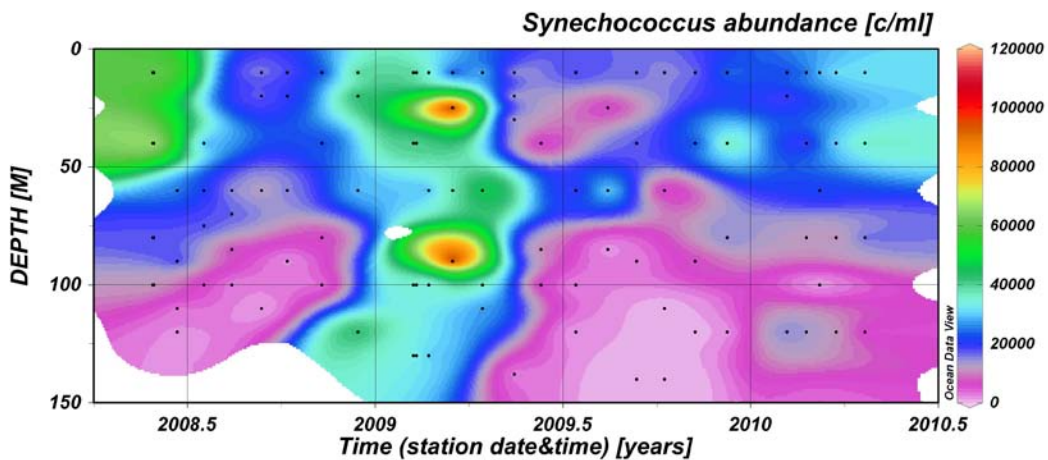


Fig. 9. Contour plot of *Synechococcus* abundance (cells mL⁻¹) from monthly and, during bloom periods, biweekly sampling at the BATS site from May 2008 to April 2010, as determined by epifluorescence microscopy. Black dots indicate sampling points. In the time scale (x-axis), 2008.5 indicates the middle of 2008 (30 June 2008), 2009 indicates 1 January 2009, and so on.

Applying the *Synechococcus*-specific C conversion equation from Verity et al. (1992) yielded a range of 4.3 to nearly 3×10^4 pg C mL⁻¹ (November 2009, 120 m, and March 2009, 25 and 90 m, respectively). C values estimated with the Menden-Deuer and Lessard (2000) non-diatom protist equation were somewhat lower, ranging from 1.7 to approximately 7000 pg C mL⁻¹.

Prymnesiophytes tended to occur between 50 and 100 m during Year 1 and the first half of Year 2 (Fig. 10). During the spring bloom of Year 2, however, abundance was highest above 50 m (2.37×10^4 (CI: 1.86 - 3.02×10^4) cells mL⁻¹, late March 2010, 40 m), with a smaller peak at 10 m (1.60×10^4 (CI: 1.31 - 1.97×10^4) cells mL⁻¹, late February 2010). An isolated peak also occurred in May 2008;

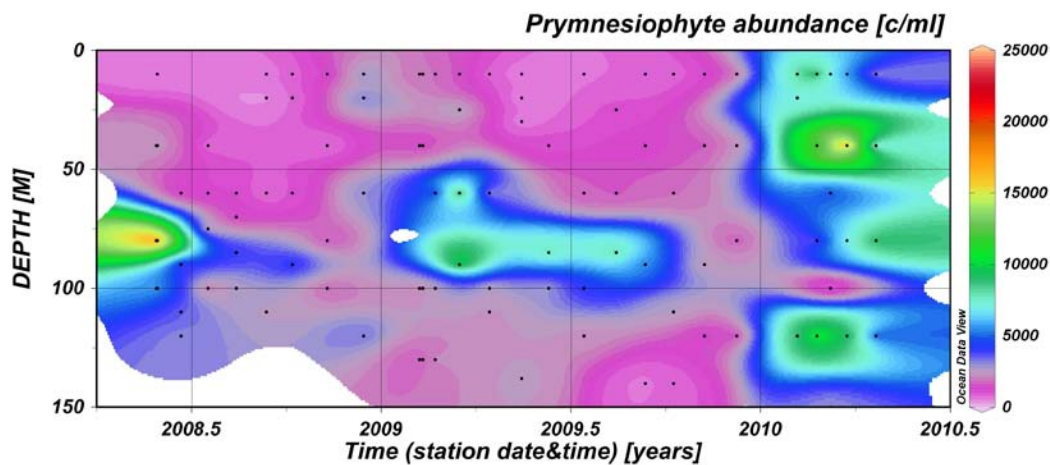


Fig. 10. Contour plot of prymnesiophyte abundance (cells mL⁻¹) from monthly and, during bloom periods, biweekly sampling at the BATS site from May 2008 to April 2010, as determined by epifluorescence microscopy. Black dots indicate sampling points. In the time scale (x-axis), 2008.5 indicates the middle of 2008 (30 June 2008), 2009 indicates 1 January 2009, and so on.

slides from two consecutive days of sampling showed $1.76\text{-}1.94 \times 10^4$ (CI: $1.32\text{-}2.34 \times 10^4$) cells mL^{-1} at 80 m. Mean cell concentration in Year 1 was lower (2904 cells mL^{-1}) than Year 2 (4005 cells mL^{-1}). The prymnesiophyte contribution to total plankton community C ranged from 14-1988 pg C mL^{-1} (mean: 1335 pg C mL^{-1}).

Prymnesiophytes in the smallest size class (1-2 μm) dominated the water column in every month of Year 2, accounting for 71-97% of average abundance (mean cells mL^{-1} of all samples in a given month) (Fig. 11). In Year 1, however, 1-2 μm cells ranged from 18-91% of all prymnesiophytes, averaging 60% (mean percent abundance of this group in Year 2 was 84%). Cells 2-4 μm in size comprised the bulk of the rest of prymnesiophyte abundance; larger cells accounted for only 0-6% of average abundance.

HNF and HDF combined abundance (Fig. 12) was greater in Year 1 than Year 2. Interestingly, combined HNF and HDF C showed an even stronger dichotomy, with total cell biomass decreasing sharply after December 2008; after this time, large cells ($>15 \mu\text{m}$) appeared less frequently (Fig. 13). In both years, abundance of these organisms was greatest from mid-summer through the end of the calendar year and lowest during the bloom. The highest cell concentration was reached in December 2008 (3271 (CI: 2302-4629) cells mL^{-1} , 60 m), while minimum abundance occurred in late February 2009 (249 (CI: 206-299) cells mL^{-1} , 60 m). HNF and HDF were relatively evenly distributed throughout the upper water column until the beginning of 2009, after which point abundance was somewhat higher in the upper 100 m.

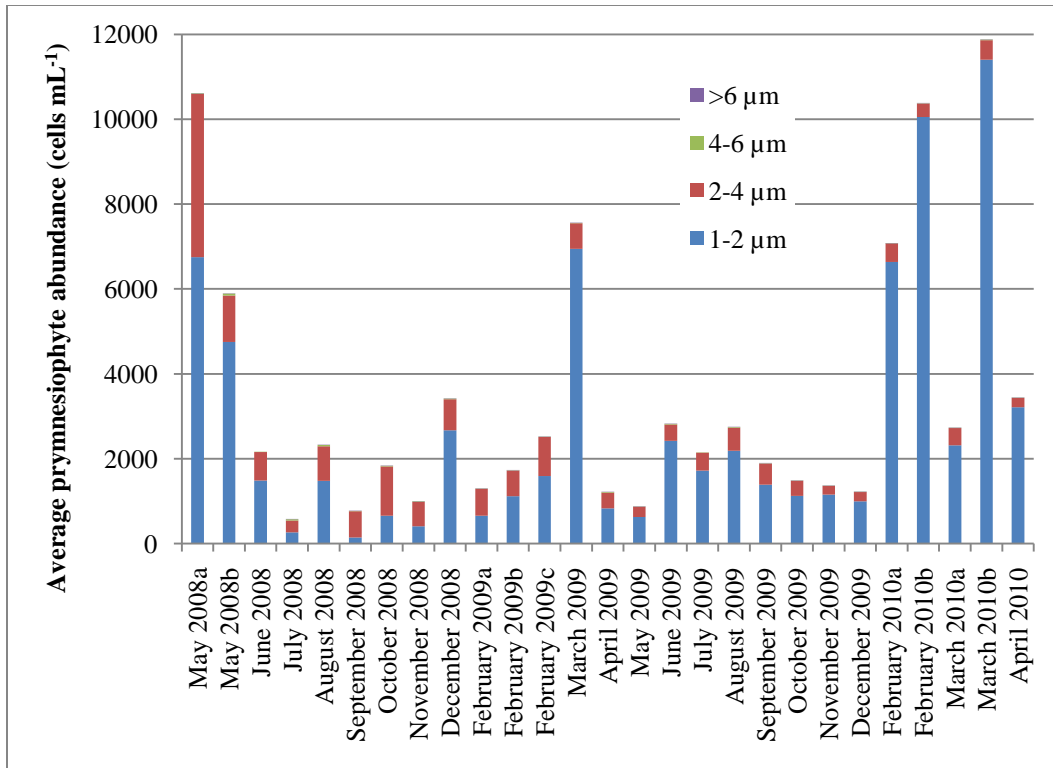


Fig. 11. Average prymnesiophyte abundance (cells mL⁻¹) per month, May 2008-April 2010. Coloration indicates abundance contributions of different size groups, with groups stacked from largest (top of bar) to smallest (bottom of bar). Cells larger than 4 μm were rarely seen and thus contributed minimally to abundance. Two sets of samples for slides were collected in May 2008 (a and b) and February 2009 (a and b); two cruises were conducted in other months indicated with a, b, or c.

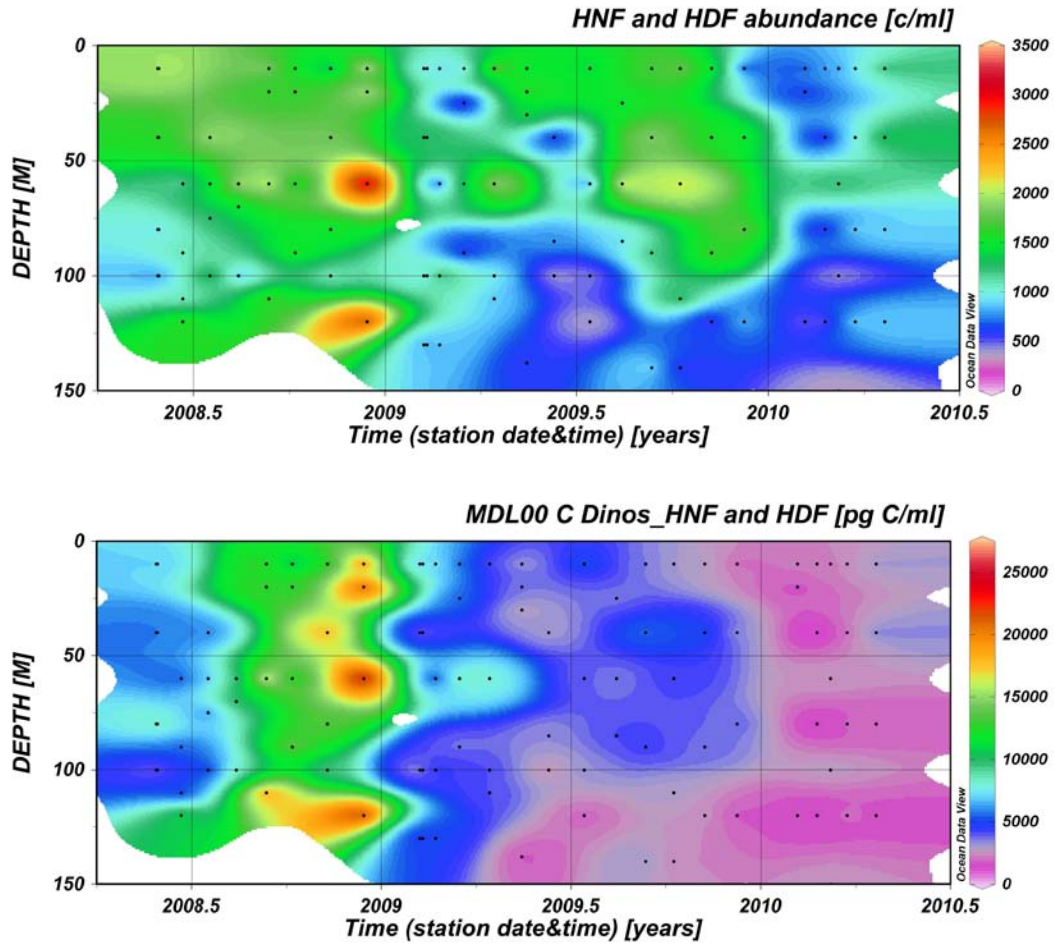


Fig. 12. Contour plot of HNF and HDF abundance (top) (cells mL^{-1}) and C (bottom) (pg C mL^{-1}) from monthly and, during bloom periods, biweekly sampling at the BATS site from May 2008 to April 2010, as determined by epifluorescence microscopy. Carbon calculated from BV using the dinoflagellate conversion equation in Menden-Deuer and Lessard (2000) (abbreviated MDL00). Black dots indicate sampling points. In the time scale (x-axis), 2008.5 indicates the middle of 2008 (30 June 2008), 2009 indicates 1 January 2009, and so on.

Average abundance of different size classes is shown in Fig. 13. HNF (cells <5 μm) dominated the community, accounting for 76-97% (mean: 91%) of average heterotrophic flagellate abundance (mean cells mL^{-1} of all samples in a given month). The smallest HDF (5-10 μm) contributed 13.1-17.5% of average HNF and HDF abundance in fall 2008 (Sept., Nov., and Dec.), but this group averaged only 5.25% of total cell concentration for the entire study period. Larger HDF were minor contributors to cell abundance, with mean abundance ranging from 0.5-1.7%. Average combined HNF and HDF abundance fell in from 1366 cells mL^{-1} in Year 1 to 1026 cells mL^{-1} in Year 2. Mean annual abundance of HNF and HDF, taken separately, also declined (from 1209 to 970 cells mL^{-1} for HNF, and from 158 to 56 cells mL^{-1} for HDF).

MDF were significantly less abundant, and contributed less to C, than HNF and HDF throughout the sampling period. Unlike heterotrophic flagellates, MDF did not include a 1-2 μm size class, as such organisms would have been difficult to distinguish from small prymnesiophytes at such a small scale; the values reported here would therefore be underestimates if 1-2 μm mixotrophic flagellates were indeed present. In both years, MDF peaked in abundance during mid to late summer, but they were more prevalent in Year 1 (maximum of 736 (CI: 602-895) cells mL^{-1} , August 2008, 85 m) than Year 2 (290 (CI: 243-344) cells mL^{-1} , August 2009, 85 m) (Fig. 14). Abundance tended to be highest between ~50-100 m, with the exception of May 2008, during which time there was a small peak in MDF at 40 m.

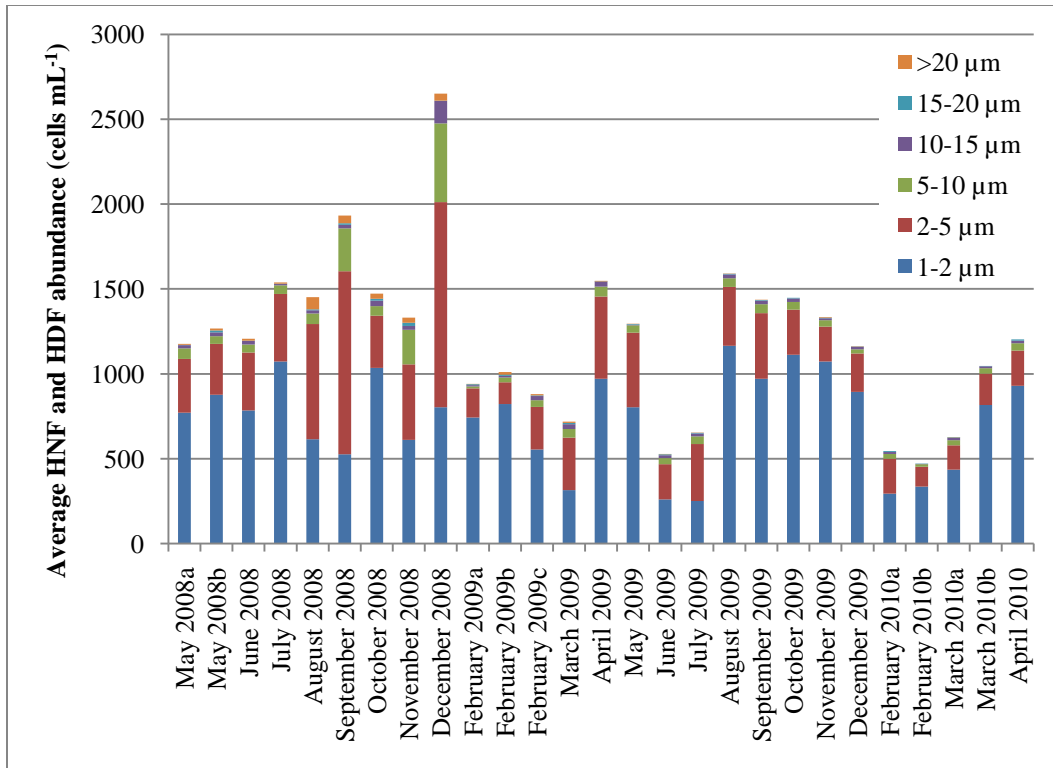


Fig. 13. Average HNF (1-5 μm) and HDF abundance (5->20 μm) (mean cells mL⁻¹ of all samples in a given month) per month, May 2008-April 2010. Coloration indicates abundance contributions of different size groups, with groups stacked from largest (top of bar) to smallest (bottom of bar). See Fig. 11 for explanation of dates (years) with a, b, or c.

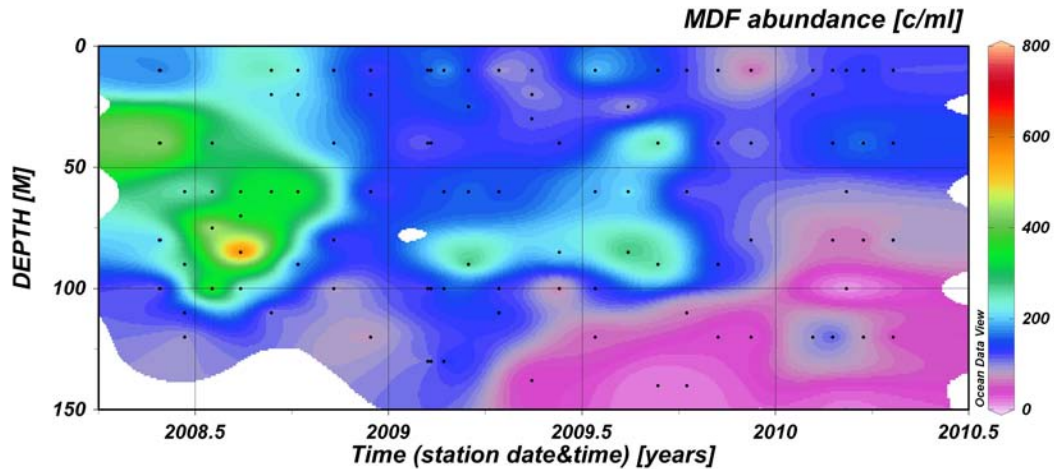


Fig. 14. Contour plot of MDF abundance (cells mL⁻¹) from monthly and, during bloom periods, biweekly sampling at the BATS site from May 2008 to April 2010, as determined by epifluorescence microscopy. Black dots indicate sampling points. In the time scale (x-axis), 2008.5 indicates the middle of 2008 (30 June 2008), 2009 indicates 1 January 2009, and so on.

As was seen in the heterotrophic flagellates, small cells dominated the MDF portion of the plankton community (Fig. 15). The 2-5 μm size class accounted for 41-87% (mean 67%) of total MDF abundance (summed cells mL⁻¹ from each sample in a given month), and the average contribution of 5-10 μm cells was 25%. The largest cells (>15 μm) were more commonly seen in Year 1 than Year 2.

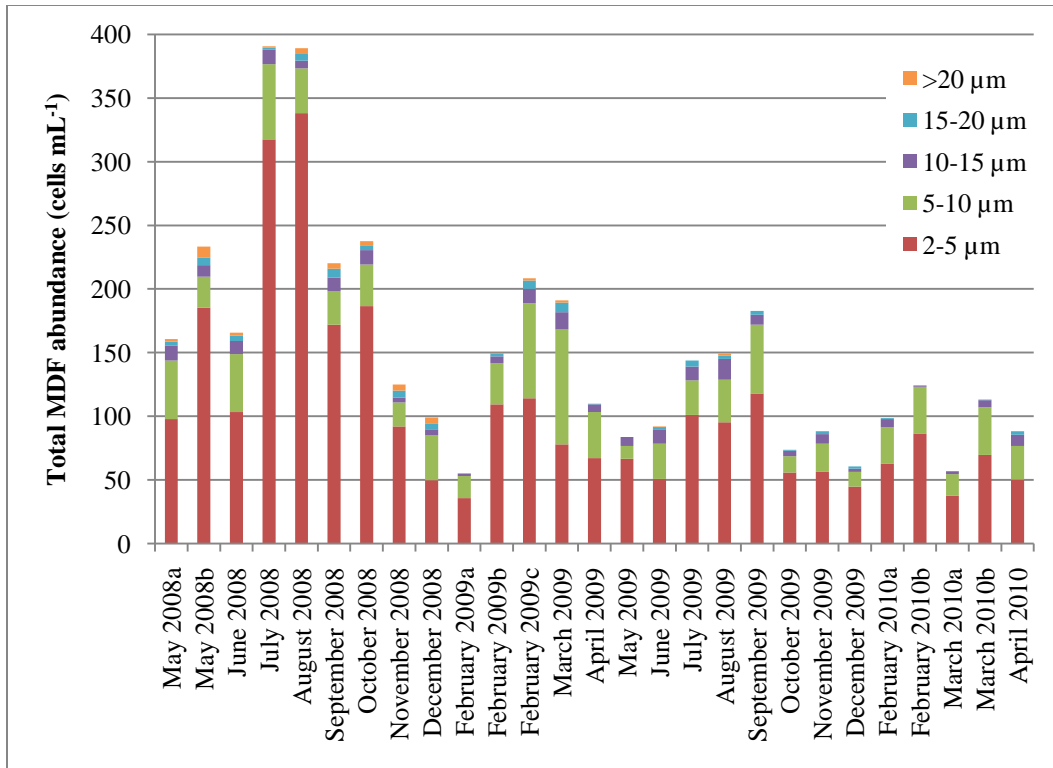


Fig. 15. Total MDF abundance (2->20 μm) (mean cells mL⁻¹ of all samples in a given month) per month, May 2008-April 2010.

Coloration indicates abundance contributions of different size groups, with groups stacked from largest (top of bar) to smallest (bottom of bar); unlike HNF, no 1-2 μm MDF were counted because such cells would have been indistinguishable from prymnesiophytes. May 2008b, June 2009 and August 2009 are sums of MDF at only three depths; the prior was not originally separated into size classes (and was later too bleached to remedy this error), and the latter two were too bleached to count (see Appendix B). See Fig. 11 for explanation of dates (years) with a, b, or c.

Diatoms were a minor taxon relative to the abundances of the groups described above, with concentrations ranging from 0 to 100 (CI: 57-111) cells mL⁻¹. Pennate diatoms comprised the bulk of overall diatom numbers, although centric diatoms experienced a brief peak in late May 2008 (Fig. 16). Diatoms tended to be found between 50-100 m. These organisms were relatively rare during the Year 1 bloom but occurred in greater densities during the Year 2 bloom. Diatom size varies immensely, from the petit *Minidiscus* (3-5 µm) (which, though known to be a common organism in the Sargasso Sea (Lomas et al. 2009b), could not be distinguished in epifluorescence counts in this study) to pennate cells 80 µm or more in length. Because a single large cell in any particular sample can dramatically skew the data at that point, it is more instructive to view diatom trends in abundance rather than in terms of BV or C.

Cryptophytes, although not traditionally considered a group of interest at BATS, nonetheless displayed interesting seasonality (Fig. 17). This taxon was relatively abundant from late winter through spring of both Years 1 and 2, at which times cells were found throughout the upper water column; however, cryptophytes were rarely seen in summer or fall. They reached peak abundance (143 (CI: 111-183) cells mL⁻¹, December 2008, 120 m) earlier in Year 1 than in Year 2 (119 (CI: 90-156) cells mL⁻¹, early February 2010, 120 m). Cryptophyte C in a given sample ranged from 0-700 pg C mL⁻¹.

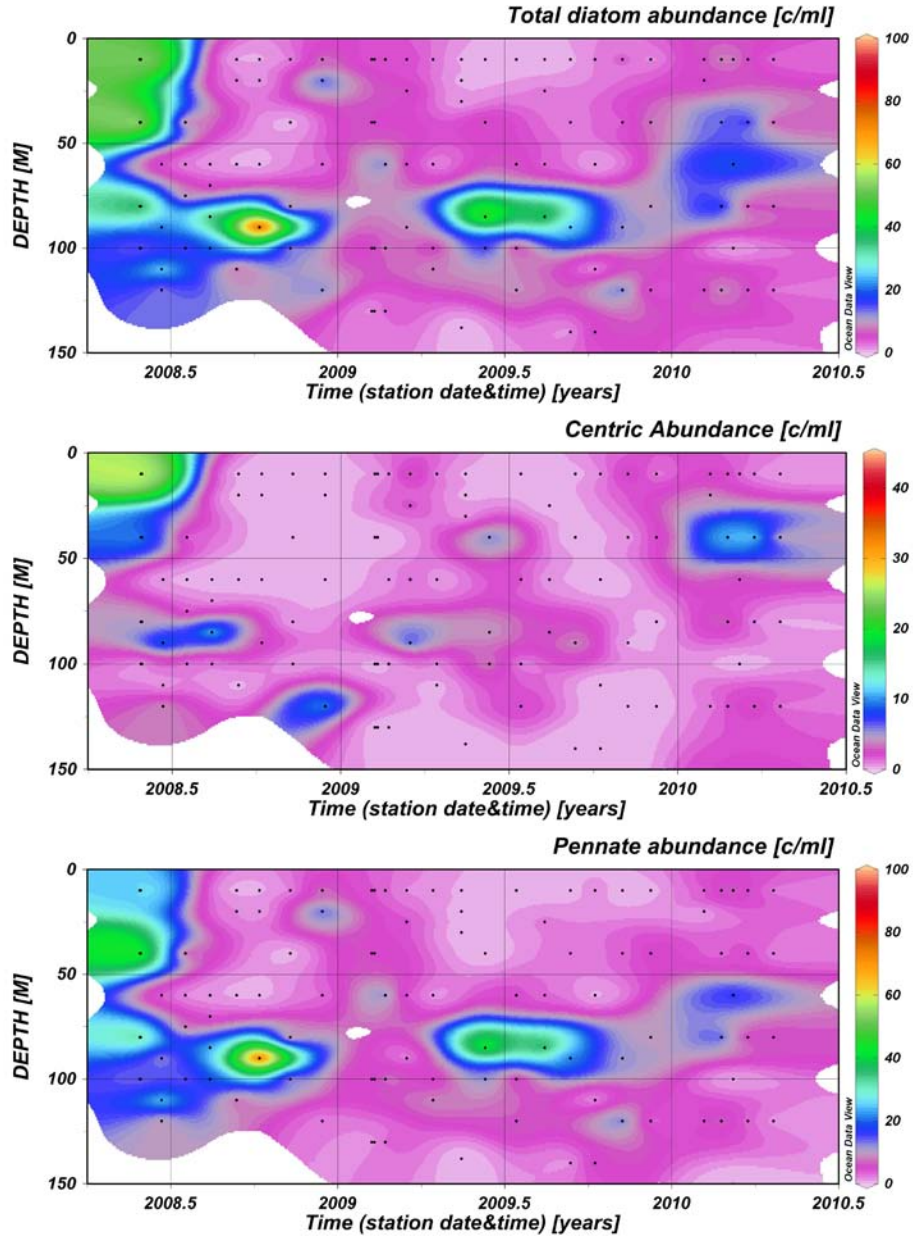


Fig. 16. Contour plots of total (top), centric (middle), and pennate diatom (bottom) abundance (cells mL⁻¹) from monthly and, during bloom periods, biweekly sampling at the BATS site from May 2008 to April 2010, as determined by epifluorescence microscopy. Black dots indicate sampling points. In the time scale (x-axis), 2008.5 indicates the middle of 2008 (30 June 2008), 2009 indicates 1 January 2009, and so on.

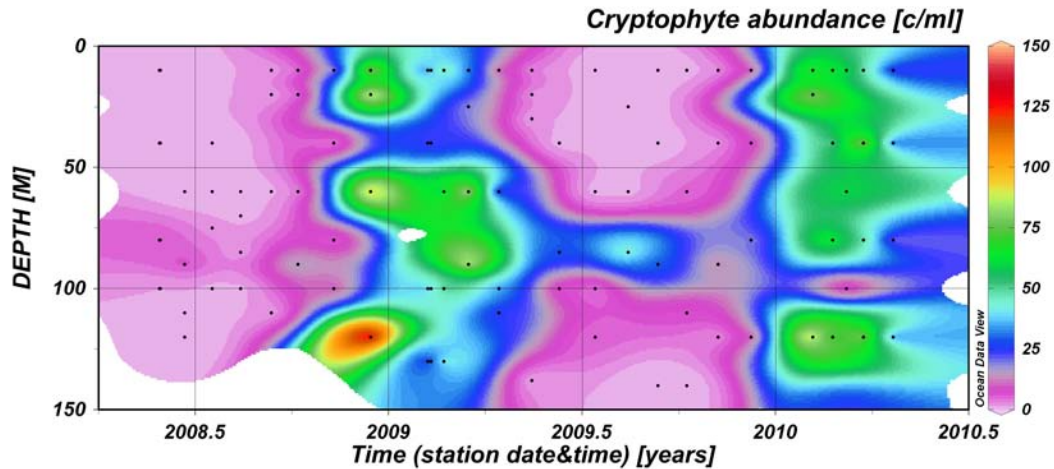


Fig. 17. Contour plot of cryptophyte abundance (cells mL⁻¹) from monthly and, during bloom periods, biweekly sampling at the BATS site from May 2008 to April 2010, as determined by epifluorescence microscopy. Black dots indicate sampling points. In the time scale (x-axis), 2008.5 indicates the middle of 2008 (30 June 2008), 2009 indicates 1 January 2009, and so on.

Fig. 18 depicts integrated C from 0-150 m, calculated from slide data with the equations provided in Menden-Deuer and Lessard (2000). Year 1 exhibited higher total integrated C than Year 2 in all months except August 2008 and one sample set from the early February 2009 cruise. Variability in the contribution of HDF explains much of the overall variability seen in Year 1. This group saw a decrease in abundance and a sharp decline in C in Year 2 (see Fig. 12), accounting for its lessened variability and contribution to total integrated C from May 2009 to the end of the study period.

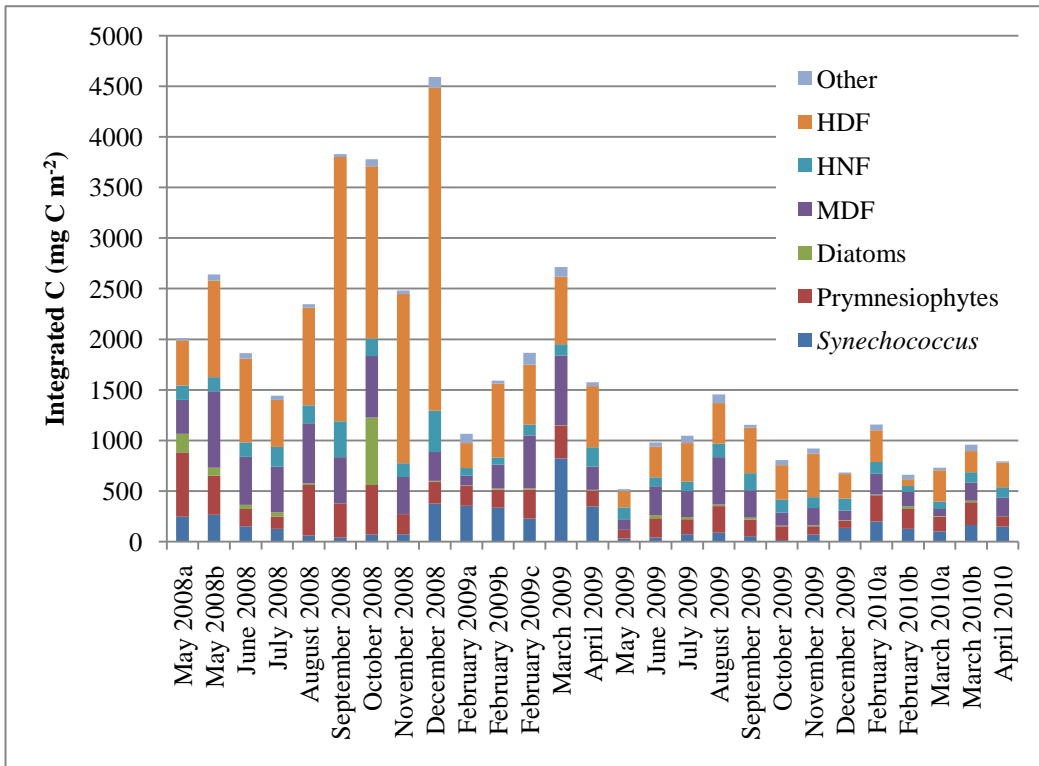


Fig. 18. Integrated C per month (mg C m^{-2}) from 0-150 m, May 2008-April 2010. Coloration indicates integrated C contributions of different taxa, with groups stacked according to trophic type (from bottom: autotrophs (*Synechococcus*, prymnesiophytes, diatoms), mixotrophs (MDF), heterotrophs (HDF, HNF), other (ciliates, cryptophytes, phototrophs, and other rarer cells). Large cells in the “diatoms” and “other” categories (i.e. with $\text{BV} > 1,000 \mu\text{m}^3$) were removed from calculations as outliers. See Fig. 11 for explanation of dates (years) with a, b, or c.

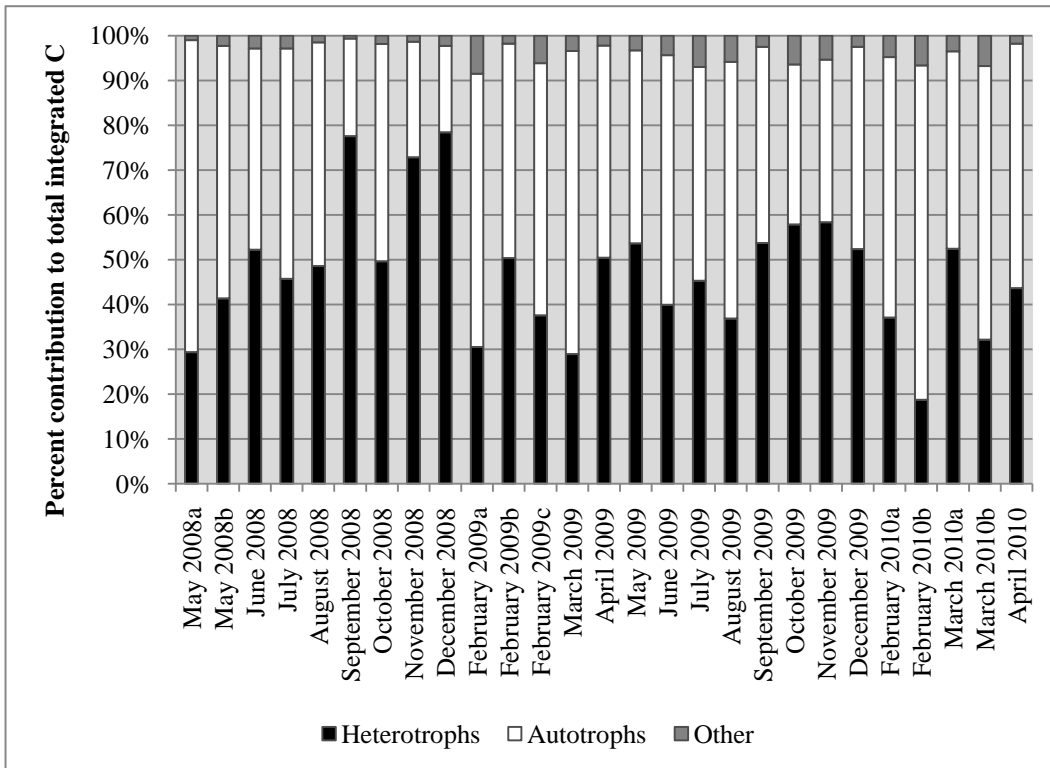


Fig. 19. Percent contributions of different groups to integrated C per month, May 2008-April 2010. Dark gray shading (top) indicates “other,” white shading (middle) indicates autotrophs, black shading indicates heterotrophs. See Fig. 18 for explanation of which taxa are “other,” autotrophs, or heterotrophs; for this analysis, MDF were classified as autotrophs. See Fig. 11 for explanation of dates (years) with a, b, or c.

The fluctuation in the relative contributions of autotrophs and heterotrophs to total integrated C (Fig. 19) shows less contrast between Years 1 and 2 than total integrated C. Heterotrophs (HNF and HDF; ciliates were included in “other” or, in many cases, were excluded from calculations as outliers due to their large size) displayed three peaks in which they reached 70% to nearly 80% of total integrated

C in fall and early winter of Year 1. While the heterotrophic contribution to C was also highest during these seasons of Year 2, these organisms then accounted for just approximately 50-60% of the total. By contrast, autotrophs dominated the community in terms of integrated C during bloom periods. The phytoplankton reached the highest percentage of total integrated C (about 75%) in late February 2010.

Scatter plots of the relationship of integrated Chl *a* ($\text{mg Chl } a \text{ m}^{-2}$) to integrated autotrophic C are shown in Fig. 20. MDF were excluded from the lower plot because these organisms may contain relatively little Chl *a* relative to their cell size, particularly for those in the larger size classes. The correlation between these values had an R^2 value of 0.10 when MDF were included in calculations of total integrated autotrophic C, and 0.17 when MDF were excluded. In neither case was there a significant relationship between integrated Chl *a* and integrated autotrophic C ($n=19$, $p=0.189$ and $p=0.080$ with and without MDF, respectively).

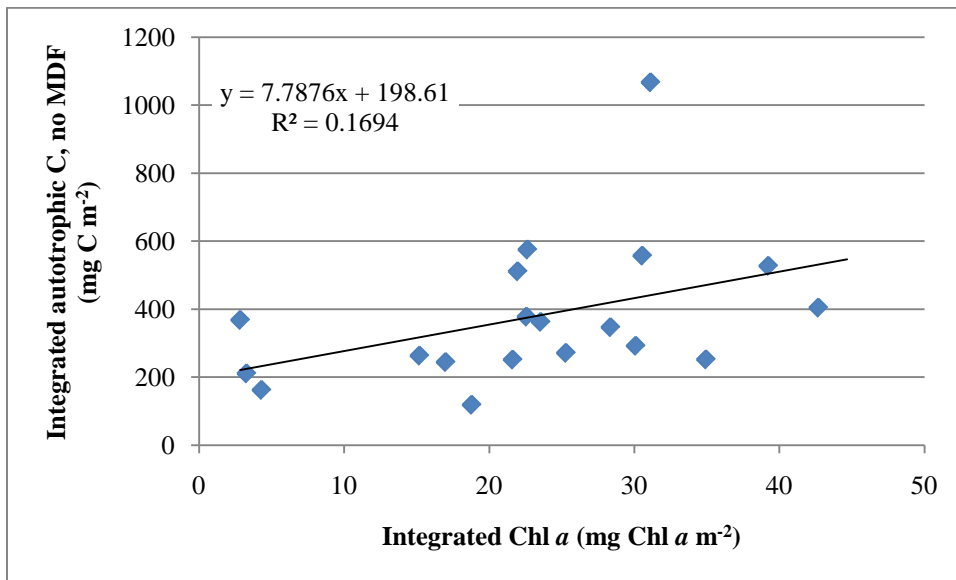
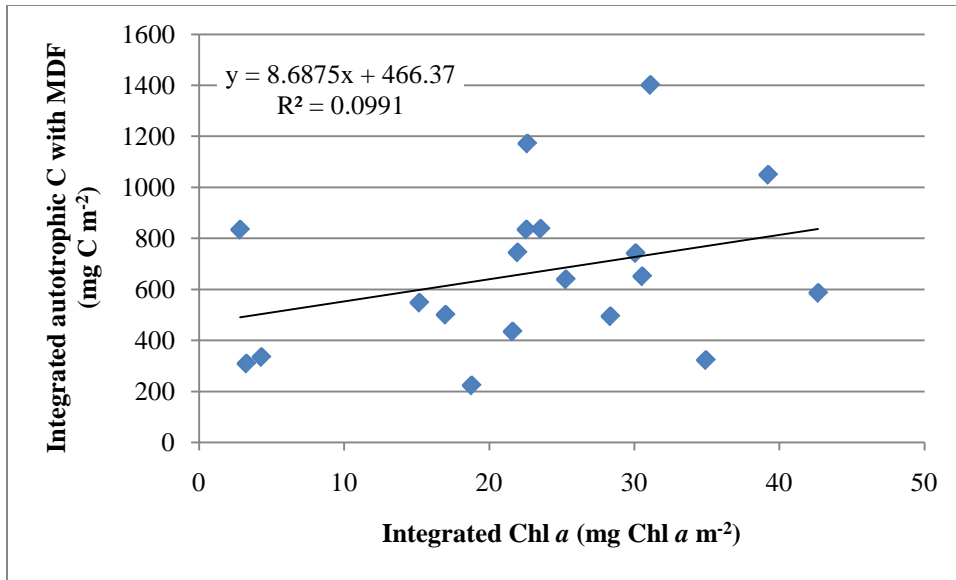


Fig. 20. Relationship of integrated Chl *a* (mg Chl *a* m⁻²) to integrated autotrophic C (mg C m⁻²) calculated from epifluorescence microscopy data of autotrophic organisms, including (top) and excluding (bottom) MDF. Data are from May 2008-April 2010. Equations and R² values for both plots are shown on the respective graphs.

DISCUSSION

All taxonomic groups surveyed in this research displayed moderate or overt temporal and spatial variability. A considerable dichotomy existed between the two study years; this was perhaps most apparent in trends in integrated C. Most autotrophic groups increased in abundance and contribution to overall C during the spring bloom; this is to be expected, as the bloom period provides the combination of adequate nutrient concentrations and light phytoplankton need to flourish. The heterotrophs studied were, by contrast, least prevalent during these bloom periods. Hydrographic variability is a strong indicator of some of the underlying causes of this planktonic variability.

Thermal stratification, or shoaling of the thermocline in summer and fall, coincided in both years with low surface Chl *a* concentrations. An interesting feature in the Year 1 thermocline that was mirrored in Chl *a* concentrations was a shoaling of ~50 m above June 2008 conditions from July to late fall. This indicates the passage of a cyclonic eddy, which causes doming of the thermocline (McGillicuddy et al. 2007). July 2008 saw an increase in all measured nutrients except nitrite (which did not increase but shoaled ~20-40 m relative to June 2008).

Another climatic event that influenced BATS hydrography occurred near the end of the study period. The winter of Year 2 “was characterized by record persistence of the negative phase of the... NAO” (Cattiaux et al. 2010, p.1), and this negative NAO explains the increased storm activity that led to deeper mixing in Year 2 (Fig. 2). Chl *a* was greater in the Year 2 bloom, and water temperature

was colder during this time. Indeed, the 18°C subtropical mode water underlying the BATS site, which is only rarely ventilated into the upper 100 m of the water column (Cianca et al. 2007), reached or nearly reached the surface (8 m was the first recorded depth) in late February 2010. The chlorophyll maximum, which previously had rested between ~100-130 m, was found between 1-60 m for much of the Year 2 spring bloom, possibly due to the high abundances of picoeukaryotes and prymnesiophytes at these depths. A surprising peak in integrated Chl *a* was seen in early April 2010, when values shot up from ~30-40 mg Chl *a* mL⁻¹ in March to >80 mg Chl *a* mL⁻¹, before decreasing to 20 mg Chl *a* mL⁻¹ two weeks later during the late April 2010 cruise. Relatively high Chl *a* values were registered at individual depths from 40-140 m (0.46-0.84 mg Chl *a* m⁻³), indicating that this peak was not the result of a single outlying measurement. FCM and primary production data are available for this cruise, but samples for epifluorescence slides were not taken.

Trends in Chl *a* were also correlated with primary production. The latter was, like Chl *a*, highest during bloom periods. The abrupt peak in integrated Chl *a* in early April 2010 did not, however, correspond to primary production maxima; production was high from 0-40 m (4.9-12.9 mg C m⁻² d⁻¹) at this time, but dropped sharply to 0-0.70 mg C m⁻² d⁻¹ below 60 m, where Chl *a* was highest. The upper region of the water column boasts high levels of both nutrients and light during these periods, however, so it is not surprising that production was highest above 40-50 m. More unexpected was the isolated peak in primary productivity seen in mid-2009 at 60 m. Chl *a* also increased slightly at that time

relative to the previous month. It could be that, as this depth was just below the heavily thermally stratified upper region, light and nutrients were still adequately sufficient to permit a brief flush of productivity. *Prochlorococcus* may have contributed to the peak in primary productivity, as this organism was most abundant in the summer and it displayed relatively high abundance from approximately 60-100 m in July 2009. Picoeukaryotes, as estimated by FCM, experienced a sudden, isolated increase in abundance at this time and depth, but this was not reflected in epifluorescence data. Both prymnesiophyte and diatom concentrations appeared elevated at ~80 m but not 60 m, the depth of the Chl *a* peak. However, samples for slides that month (July 2009) were collected at 10, 60, 100, and 120 m, and the abundance increases at ~80 m are extrapolated from data from 85 m slides taken in June and August 2009.

Numerous relationships between Chl *a*, FCM data for pico- and nano-eukaryotes, and epifluorescence data, both throughout the upper water column and over time, can be illuminated by delving into these data. At the very beginning of the study period in May 2008, an unusual peak (unusual because it occurred after the spring bloom, at the beginning of thermal stratification) in Chl *a* was observed between approximately 75-100 m. This coincided with a marked abundance of picoeukaryotes (and, to a lesser extent, nanoeukaryotes) in the FCM data. Prymnesiophytes, as observed by microscopy, also exhibited high concentrations at this depth in May. Thus, these are most likely the organisms seen in the FCM data. This provides a noteworthy example of how microscopy data can be supported by evidence from high-throughput techniques like FCM,

and FCM can benefit from the more precise degree of identification afforded by microscopy. Unlike this peak in prymnesiophytes, the abundance of diatoms between 0-50 m noted in slide counts in May 2008 was not reflected in Chl *a* data, although FCM nanoeukaryote results show a high concentration of cells in the upper 10-20 m.

FCM data somewhat explain the peak in integrated Chl *a* that occurred in early April 2010. *Prochlorococcus* most likely had a minimal impact on Chl *a* at that time, given that this organism was at its lowest concentrations in the Year 2 spring bloom. Instead, *Synechococcus* may have contributed, although Chl *a* is not this cyanobacterium's primary light-harvesting pigment. *Synechococcus* concentrations were high ($2.29\text{-}3.34 \times 10^4$ cells mL⁻¹) from 0-40 m, but they dropped at 60 m to 8.22 cells mL⁻¹ and continued to decline deeper in the water column, where Chl *a* concentrations were highest. Photosynthetic nanoeukaryotes were high relative to typical abundances in the upper 40 m (129-225 cells mL⁻¹) but as low as 15 cells mL⁻¹ below that; however, these organisms contain more Chl *a* than the smaller picoeukaryotes by virtue of their size, so this may partially explain the Chl *a* peak. It seems most likely that picoeukaryotes were responsible for that peak, given their dense concentrations (up to 6640 cells mL⁻¹) in early April in the upper 80-100 m—although abundances were actually greater in late March—and it is equally likely that small prymnesiophytes comprised the bulk of this picoeukaryotic population.

Prymnesiophyte abundance, as estimated by microscopy, correlated strongly with Chl *a* data throughout the study. Prymnesiophytes were the most

prevalent chlorophyll-containing taxon seen in slide counts; *Synechococcus* contains a different main accessory pigment, and the chlorophyll-containing MDF and diatoms were much less abundant. Liu et al. (2009) recently published a major finding, resulting from HPLC studies of the haptophyte pigment 19'-hexanoyloxyfucoxanthin (19-Hex), that prymnesiophytes (the Haptophyta) are a dominant eukaryotic phytoplankton throughout the world's open oceans. These authors also used molecular techniques to reveal that prymnesiophyte populations are characterized by an extremely high degree of diversity. Given these organisms' morphological similarity, however, such diversity cannot be uncovered in microscopy analyses.

It is worth noting that the size classes used in this study to categorize prymnesiophytes (and HNF, HDF, and MDF) do not necessarily correspond to different species. The incredible dominance of 1-2 μm prymnesiophytes during bloom periods could indicate an abundance of a small haptophyte species; alternatively, these cells could be recently divided progeny that have not yet reached their full size. Also worthy of note is the consideration that the centric diatom *Minidiscus*, known to be abundant in many plankton communities but difficult to identify by light microscopy (Hasle and Syvertsen 1997), could hypothetically have been included in the 2-4 μm prymnesiophyte size class. However, a whitish or green silica frustule (shell) would likely have been visible around the cells, as clearly observed in the other centric diatoms observed by epifluorescence in this study, and this was not seen in any slide counts. Coccolithophores are known to occur in the BATS region, but they only comprise

a portion of the prymnesiophyte (haptophyte) community. Haidar and Thierstein (1995) reported cell abundances of coccolithophorid species as high as 106×10^3 cells L^{-1} ($106 \text{ cells mL}^{-1}$), with mean density around 20×10^3 cells L^{-1} . In contrast, epifluorescence microscopy revealed mean prymnesiophyte concentrations an order of magnitude higher; the mean coccolithophore concentration found in Haidar and Thierstein's study would comprise less than 1% of all prymnesiophytes at or near the BATS station.

Unlike prymnesiophytes, *Synechococcus* is not a major contributor to Chl *a*, as these cells instead contain phycobiliproteins like phycocyanin and phycoerythrin (though Chl *a* is still present, predominantly in the cells' reaction centers) (Collier and Grossman 1992). Instead, it must be charted by other techniques, such as molecular methods or the techniques employed in this study. Spatial and temporal trends in abundance of *Synechococcus* were mirrored in FCM and slide results. Both showed peaks in concentrations of the cyanobacterium in May 2008 in the upper 75 m, in the spring bloom of Year 1 throughout the upper 150 m, and in the bloom of Year 2 in the upper 50-75 m of the water column.

Estimations of *Synechococcus* abundance were, however, greater by approximately a factor of two in epifluorescence data than in FCM data; this was also true for slide count prymnesiophyte estimates when compared to picoplankton abundances from FCM. There are several possible explanations for this discrepancy. First, slide samples and FCM samples may not have been collected at the same time or on the same day of each cruise; this would account

for some differences in determined abundance if cell concentrations varied somewhat from day to day, but it would not explain the consistent difference in overall concentration. It is also possible that variations existed in the precise diameter of the glass columns used for at-sea filtration of microscopy samples. Even a difference of <1 mm in column diameter would impact the filter area, correspondingly skewing the field-specific conversion factors used to translate microscopy counts into cell abundances. If FCM estimates were indeed closer to actual cell concentrations, and if the filtration columns used on the ship were slightly smaller than those used to calculate the aforementioned conversion factors, then that could partially account for the possible systematic error noted above. Furthermore, both techniques are also prone to subsampling error, though FCM may be more at risk for this due to the small amount of sample (generally ~0.2-0.3 mL) used in processing (Lomas et al. 2009b). Error in estimating cell abundance can be quite large when only a few cells of a certain organism or taxon are counted by microscopy (e.g. approximately $\pm 100\%$ if 4 cells are counted, $\pm 50\%$ if 16 cells are counted, assuming 95% confidence limits (Lund et al. 1958)). However, *Synechococcus* and picoeukaryotes (predominantly prymnesiophytes) were common enough to count 30-100 cells or more in almost all samples (with the exception of several slides, especially some below ~120 m) to achieve a reasonable margin of error (approximately $\pm 30\%$ error for 30 cells, $\pm 20\%$ for 100 cells).

Prochlorococcus dynamics cannot be compared between the two techniques because this organism is difficult or impossible to see with

epifluorescence microscopy. Based on FCM data, *Prochlorococcus* was seen in the greatest numbers during summer and fall, a finding in line with that of DuRand and colleagues (2001). These researchers also noted that *Synechococcus* is most prevalent during the spring bloom, a result echoed here. The present study, however, goes further in illustrating the dynamics of these cyanobacteria at the BATS site by elucidating their spatial structure in the upper water column. It is shown here that *Synechococcus* is most abundant in the upper 100 m of the surface ocean, while *Prochlorococcus* is generally found between 50-100 m.

Other phytoplankton—MDF, diatoms, cryptophytes, and rarer organisms like ciliates and unclassified phototrophs—likewise exhibited distinct seasonality. MDF reached peak abundances during bloom periods, primarily between 50-100 m. Interannual variability was also clear in this group, with abundances, especially of cells in the larger size classes, decreasing in Year 2. Cryptophytes, though low in abundance overall (less than approximately $150 \text{ cells mL}^{-1}$), also followed a bloom pattern of seasonality, with concentrations peaking in late winter and during the early period of the spring bloom. These cells were almost or completely absent throughout the water column at other times of both Years 1 and 2. Diatom abundance, however, did not strictly coincide with the spring bloom. Concentrations of these organisms, both pennate and centric, were highest in May 2008 and in summer to fall of 2008 and 2009, largely between 50-100 m. Diatoms were seen in both spring blooms, with greater spatial distribution (~10-80 m) but lower concentrations than in other seasons. Abundance slightly increased in the Year 2 bloom relative to that of Year 1, but since these organisms were relatively

rare, they bring with them the baggage of a noteworthy degree of counting error. The abrupt diatom abundance peak in October 2008 did not correlate with any recorded injection of silicate into the upper water column; an earlier eddy had led to increased levels of this compound from ~100-200 m, but that event occurred in July 2008.

Heterotrophic flagellate seasonal dynamics were opposite those of most phytoplankton. Populations of these microbes were largest in late summer to early winter, and they shrank as the spring bloom began. A recent article published by Behrenfeld (2010) proposed a “Dilution-Recoupling Hypothesis” to replace the “Critical Depth Hypothesis” proposed by Sverdrup in 1953, and this new hypothesis may shed some light on the importance of HNF and HDF dynamics seen here. Sverdrup’s paradigm holds that the spring bloom is set in motion when, after deep mixing in winter, the nutrient-replete MLD shoals above the critical depth horizon, which is the depth at which phytoplankton growth is less than biomass loss through respiration, sinking, or grazing; thus, the bloom occurs due to hydrographic conditions that allow increased cell growth. However, Behrenfeld presented a multi-year data set from the North Atlantic showing that, among other things, phytoplankton C actually begins to increase in mid-winter rather than in spring. He concluded that increased cell division cannot account for the timing and dynamics of the bloom. Rather, decreased predation occurs in mid-winter due to dilution as the MLD deepens. Grazing is “recoupled” to phytoplankton growth when the MLD shoals, but the hydrographic conditions listed above allow autotrophic growth rates to remain high despite increases in predation.

Although increased light conditions in spring play a minor role in bloom control in the subtropics compared to polar regions, it is still possible that Behrenfeld's hypothesis could hold true at BATS and similar areas. The decrease in concentrations of grazers (HNF and HDF in this study, though possibly not that of ciliates (see below)) noted in late winter and early spring of both Years 1 and 2 lends credence to the idea that low predation could indeed spark the spring bloom, since the heterotrophic flagellates are primary grazers of the BATS phytoplankton community. Preliminary data from A. Freibott, a colleague investigating ciliate taxonomy and dynamics from BATS samples taken concurrently with those of the present study, suggests that ciliate concentrations increased throughout the water column during the bloom of Year 1, although these heterotrophs also exhibited relatively high abundance below 100 m from May 2008 through summer and fall 2008. Like HNF and HDF, ciliate abundance fell in Year 2, and an increase in prevalence of these organisms was not seen in the second spring bloom. Lessard and Murrell (1996) reported ciliate concentrations markedly lower than those of HDF, a finding also seen here: high ciliate concentrations from A. Freibott's study ranged from ~500-800 cells L⁻¹, or <1 cell mL⁻¹, drastically lower than even the lowest concentration of HNF and HDF (249 cells mL⁻¹) calculated from slide counts.

HNF and HDF also displayed interannual variation. This was most pronounced in the difference in HNF/HDF C between Year 1 and Year 2, with C plunging in early 2009 before falling still lower by May 2009 (the beginning of Year 2). The drop in prevalence of large cells (particularly those >15 μm) at the

beginning of Year 2 accounts for much of this difference in C, but lessened overall abundance in that year also contributed.

An astonishing range of C conversion factors for phytoplankton and heterotrophic protists is available in the literature. For this study, one set of equations—those provided by Menden-Deuer and Lessard (2000)—was chosen for its relevance to this work (chiefly, the provision of a separate dinoflagellate equation, the recognition of diatoms as containing less C than most protists due to their large vacuole, and the simplicity afforded by applying a single equation to other protists). Furthermore, that study is well regarded in the fields of phycology and oceanography, based on the number of citations it has garnered in the past decade. Estimating plankton C is, however, a notoriously error-prone business, not least because preserved or “fixed” cells may not precisely reflect the size or shape of live organisms.

Fixation of filtered plankton with glutaraldehyde is indisputably necessary, as on-ship facilities for examining live samples are not available. However, glutaraldehyde and other fixatives are known to induce shrinkage of microscopic organisms. Choi and Stoecker (1989) found that 2% glutaraldehyde resulted in approximately 42-45% shrinkage over live volume of microflagellates, approximately 54-64% shrinkage of naked ciliates, and approximately 76% shrinkage of a loricated ciliate. These percentages indicate the size of the fixed cells relative to their original live volume. Autotrophic flagellates generally shrink less than heterotrophic ones, possibly because phagotrophs may release ingested particles upon contact with a fixative (Choi and Stoecker 1989). Booth (1987) and

Verity et al. (1992) found average volume reductions of 28% and 29% with 2.5% and 0.5% glutaraldehyde, respectively.

Menden-Deuer and Lessard (2000) noted that the effects of fixation vary widely between species and can, in some cases, also cause swelling of cells. These authors concluded that C to volume conversion equations are nevertheless applicable to both live and dead cells. The extensive variability of fixative-induced shrinkage makes it difficult, if not impossible, to accurately correct the dimensions and BV of fixed cells. It must therefore be assumed that the BV and C conversion data presented here are underestimations of live-cell BV and C, perhaps of at least 30%.

This study reveals that plankton communities in the NASTG are subject to a great degree of spatial and temporal variability in terms of taxonomic composition, size makeup of the community, the ratio of autotroph to heterotroph biomass, and total integrated C. Moreover, hydrography and climate forcing—whether relatively brief mesoscale events (such as storms or passing eddies), recurring seasonal and regional events (as in the case of the spring bloom), or long-term hemispheric or global events (like fluctuations in the NAO or global climate patterns)—have mild to acute effects on the microbial community.

Despite this hydrographic variability, the consistently oligotrophic nature of the BATS site becomes abundantly clear upon perusal of the trends in nutrient availability. Concentrations of nitrite tended to be lowest throughout the water column, and PO_4 and nitrate were minimal above 100 m, making it seem possible that these nutrients play interchanging roles as limiting nutrients. Although no

nutrient data are available past March 2009, it is probable that the injection of nutrients into the upper water column was more intense preceding the Year 2 bloom than that of Year 1, given the greater Chl *a* values and phytoplankton abundances seen in 2010.

The most curious paradox exposed in this research regarding interannual variability was the way in which Chl *a* values increased in the second year, especially during the bloom season, but integrated C plummeted. Logically, Chl *a* should have decreased in conjunction with C, because one would assume that less C, or less cell biomass, would correspond to fewer phototrophic cells. But prymnesiophytes—the largest phototrophic taxon followed in the present study—actually increased in Year 2. How, then, can this mysterious contradiction be explained? In fact, there are multiple factors that contributed to the decrease in C but concurrent increase in Chl *a*. Fewer heterotrophs (HNF and HDF), especially large heterotrophs that contribute disproportionately to total planktonic biomass relative to their abundance (Lessard and Murrell 1996), were found in Year 2. This had a striking influence on integrated C. MDF also decreased after Year 1, with a corresponding impact on total C (though to a lesser degree than HDF, as MDF were much less abundant to begin with). Because chloroplasts take up relatively little of the MDF cell body, a lower concentration of these organisms probably had a smaller impact on Chl *a* than it had on integrated C. The decrease in *Synechococcus* noted in Year 2 also had a larger impact on decreasing total C than it had on Chl *a* concentrations, as these cyanobacteria mainly contain other photosynthetic pigments. As noted above, prymnesiophytes (and FCM-derived

picoplankton estimates) increased in the second study year, but these tiny organisms make only a small contribution to total C. It is also possible that Chl *a* content per cell was higher in 1-2 μm prymnesiophytes than in larger cells. Finally, and regrettably, slides were not available for the highest peak in Chl *a* seen in early April of 2010, so it is impossible to know exactly which organisms in the phytoplankton community were responsible for the high chlorophyll observed during this time.

Chl *a* is often used as a proxy for phytoplankton abundance (Dierssen 2010) and is “considered a reliable indicator of both phytoplankton abundance and biomass” (Boyce et al. 2010, p. 591). The present study, however, found a weak correlation ($R^2=0.0991$ or 0.1694 if MDF are included or excluded, respectively, from integrated autotrophic C) between integrated Chl *a* and integrated autotrophic C from 0-150 m. Although there are inherent assumptions built into the calculation of integrated C from just four sampled depths, the low R^2 values and the monthly variability of the integrated autotrophic C :Chl *a* ratio (not shown) presented here suggest that Chl *a* may not be as strong an indicator as believed, at least for the BATS site.

Heterotrophic bacteria were not included in epifluorescence microscopy counts in the present study; nevertheless, previous research has revealed concentrations on the order of 10^5 cells mL^{-1} (Caron et al. 1995; Carlson et al. 2009). The SAR11 clade of the α -proteobacteria dominates the bacterioplankton, though other clades like OCS116 are also abundant. Both groups, along with other less prevalent organisms, show annual variability correlated with the region’s

hydrographic seasonality (Carlson et al. 2009; Treusch et al. 2009). The omission of heterotrophic bacteria from this study means calculations of integrated C and the relative contributions of heterotrophs and autotrophs to integrated C are necessarily underestimations of actual values.

This research and other plankton community work currently being conducted as part of BATS has implications for increasing the scientific community's understanding of biogeochemical cycles in the Sargasso Sea. C flux, or export of C to the deep ocean, is an ongoing topic of research in this region. Variations in the euphotic zone's plankton community indisputably impact the type and amount of organic material sinking to depth, an issue that has implications for climate research.

The apparent sensitivity to climate discussed above is worrisome in light of anticipated increasing ocean acidification (Orr et al. 2005; Doney et al. 2009) and climate change (Falkowski et al. 2000; Boyce et al. 2010). Phytoplankton abundance has declined globally since the Industrial Revolution, with increasing sea surface temperature related to increasing atmospheric concentrations of CO₂ and other greenhouse gases and changes in the NAO and ENSO cited as two possible causes (Boyce et al. 2010). Because the ocean also functions as a tremendously significant sink for CO₂, declines in autotrophic biomass could portend a lessened capability for marine systems to take in this greenhouse gas, leading to further increased temperatures and disrupted climate patterns in a self-perpetuating cycle (Sabine et al. 2004). Developing an understanding of the composition, seasonality, and variability of the plankton community at BATS and

time-series stations around the globe is critical if researchers hope to accurately model and predict the responses of these communities to a changing ocean.

REFERENCES

- Amacher, J., S. Neuer, I. Anderson and R. Massana. 2009. Molecular approach to determine contributions of the protist community to particle flux. *Deep-Sea Res. Pt. I.* **56**: 2206-2215, doi:10.1016/j.dsr.2009.08.007
- Booth, B. B. C. 1987. The use of autofluorescence for analyzing oceanic phytoplankton communities. *Bot. Mar.* **30**: 101-108.
- Borsheim, K. Y. and G. Bratbak. 1987. Cell-volume to cell carbon conversion factors for a bacterivorous *Monas* sp. enriched from seawater. *Mar. Ecol. Prog. Ser.* **36**: 171-175.
- Boyce, D. G., M. R. Lewis and B. Worm. 2010. Global phytoplankton decline over the past century. *Nature.* **466**: 591-596, doi:10.1038/nature09268
- Cattiaux, J. J. 2010. Winter 2010 in Europe: A cold extreme in a warming climate. *Geophys. Res. Lett.* **37**: L20704.
- Choi, J. W. and D. K. Stoecker. 1989. Effects of fixation on cell-volume of marine planktonic protozoa. *Appl. Environ. Microbiol.* **55**: 1761-1765.
- Cianca, A., P. Helmke, B. Mourino, M. J. Rueda, O. Llinas and S. Neuer. 2007. Decadal analysis of hydrography and in situ nutrient budgets in the western and eastern North Atlantic subtropical gyre. *J. Geophys. Res.* **112**: C07025, doi:10.1029/2006JC003788
- Collier, J. L. and A. R. Grossman. 1992. Chlorosis induced by nutrient deprivation in *Synechococcus* sp. strain PCC 7942: Not all bleaching is the same. *J. Bacteriol.* **174**: 4718-4726.
- Dierssen, H. M. 2010. Perspectives on empirical approaches for ocean color remote sensing of chlorophyll in a changing climate. *Proc. Natl. Acad. Sci. U. S. A.* **107**: 17073-17078, doi:10.1073/pnas.0913800107
- Doney, S. C., V. J. Fabry, R. A. Feely and J. A. Kleypas. 2009. Ocean acidification: The other CO₂ problem. *Annu. Rev. Mar. Sci.* **1**: 169-192, doi:10.1146/annurev.marine.010908.163834
- Dubinsky, Z. and N. Stambler. 2009. Photoacclimation processes in phytoplankton: Mechanisms, consequences, and applications. *Aquat. Microb. Ecol.* **56**: 163-176, doi:10.3354/ame01345

- DuRand, M. D., R. J. Olson and S. W. Chisholm. 2001. Phytoplankton population dynamics at the Bermuda Atlantic Time-series Station in the Sargasso Sea. *Deep-Sea Res. Pt. II.* **48**: 1983-2003.
- Falkowski, P., R. J. Scholes, E. Boyle, J. Canadell, D. Canfield, J. Elser, N. Gruber, K. Hibbard, P. Hogberg, S. Linder, F. T. Mackenzie, B. Moore, T. Pedersen, Y. Rosenthal, S. Seitzinger, V. Smetacek and W. Steffen. 2000. The global carbon cycle: A test of our knowledge of earth as a system. *Science.* **290**: 291-296.
- Haidar, A. T. and H. R. Thierstein. 2001. Coccolithophore dynamics off Bermuda (N. Atlantic). *Deep-Sea Res. Pt. II.* **48**: 1925-1956.
- Hasle, G. R. and E. E. Syvertsen. 1997. Marine Diatoms, p. 5-385. *In* C. R. Tomas [ed.], *Identifying Marine Phytoplankton*. Academic Press.
- Heimdal, B. R. 1997. Modern Coccolithophorids, p. 731-833. *In* C. R. Tomas [ed.], *Identifying Marine Phytoplankton*. Academic Press.
- Hillebrand, H., C. D. Durselen, D. Kirschtel, U. Pollinger and T. Zohary. 1999. Biovolume calculation for pelagic and benthic microalgae. *J. Phycol.* **35**: 403-424.
- Lessard, E. J. and M. C. Murrell. 1996. Distribution, abundance and size composition of heterotrophic dinoflagellates and ciliates in the Sargasso Sea near Bermuda. *Deep-Sea Res. Pt. I.* **43**: 1045-1065.
- Lessard, E. J. and E. Swift. 1986. Dinoflagellates from the North Atlantic classified as phototrophic or heterotrophic by epifluorescence microscopy. *J. Plankton Res.* **8**: 1209-1215.
- Liu, H., I. Probert, J. Uitz, H. Claustre, S. Aris-Brosou, M. Frada, F. Not and C. de Vargas. 2009. Extreme diversity in noncalcifying haptophytes explains a major pigment paradox in open oceans. *Proc. Natl. Acad. Sci. U. S. A.* **106**: 12803-12808, doi:10.1073/pnas.0905841106
- Lomas, M. W., F. Lipschultz, D. M. Nelson, J. W. Krause and N. R. Bates. 2009a. Biogeochemical responses to late-winter storms in the Sargasso Sea, I—Pulses of primary and new production. *Deep-Sea Res. Pt. I.* **56**: 843-860, doi:10.1016/j.dsr.2008.09.002
- Lomas, M. W., N. Roberts, F. Lipschultz, J. W. Krause, D. M. Nelson and N. R. Bates. 2009b. Biogeochemical responses to late-winter storms in the Sargasso Sea, IV—Rapid succession of major phytoplankton groups. *Deep-Sea Res. Pt. I.* **56**: 892-908, doi:10.1016/j.dsr.2009.03.004

- Lomas, M. W., D. K. Steinberg, T. Dickey, C. A. Carlson, N. B. Nelson, R. H. Condon and N. R. Bates. 2010. Increased ocean carbon export in the Sargasso Sea linked to climate variability is countered by its enhanced mesopelagic attenuation. *Biogeosciences*. **7**: 57-70.
- Lomas, M. W. and S. B. Moran. 2010. Evidence for aggregation and export of cyanobacteria and nano-eukaryotes from the Sargasso Sea euphotic zone. *Biogeosciences Discuss*. **7**: 7173-7206.
- Lund, J. W. G., C. Kipling, and E. D. Le Cren. 1958. The inverted microscope method of estimating algal numbers and the statistical basis of estimations by counting. *Hydrobiologia*. **11**: 143-170.
- McGillicuddy, D. J., Jr., L. A. Anderson, N. R. Bates, T. Bibby, K. O. Buesseler, C. A. Carlson, C. S. Davis, C. Ewart, P. G. Falkowski, S. A. Goldthwait, D. A. Hansell, W. J. Jenkins, R. Johnson, V. K. Kosnyrev, J. R. Ledwell, Q. P. Li, D. A. Siegel and D. K. Steinberg. 2007. Eddy/wind interactions stimulate extraordinary mid-ocean plankton blooms. *Science*. **316**: 1021-1026, doi:10.1126/science.1136256
- Menden-Deuer, S. and E. J. Lessard. 2000. Carbon to volume relationships for dinoflagellates, diatoms, and other protist plankton. *Limnol. Oceanogr.* **45**: 569-579.
- Mullin, M. M., P. R. Sloan and R. W. Eppley. 1966. Relationship between carbon content cell volume and area in phytoplankton. *Limnol. Oceanogr.* **11**: 307-311.
- Nelson, N. B., D. A. Siegel and J. A. Yoder. 2004. The spring bloom in the northwestern Sargasso Sea: Spatial extent and relationship with winter mixing. *Deep-Sea Res. Pt. II*. **51**: 987-1000, doi:10.1016/j.dsr2.2004.02.001
- Neuer, S. and T. J. Cowles. 1994. Protist herbivory in the Oregon upwelling system. *Mar. Ecol. Prog. Ser.* **113**: 147-162.
- Not, F., R. Gausling, F. Azam, J. F. Heidelberg and A. Z. Worden. 2007. Vertical distribution of picoeukaryotic diversity in the Sargasso Sea. *Environ. Microbiol.* **9**: 1233-1252, doi:10.1111/j.1462-2920.2007.01247.x
- Not, F., M. Latasa, R. Scharek, M. Viprey, P. Karleskind, V. Balague, I. Ontoria-Oviedo, A. Cumino, E. Goetze, D. Vaultot and R. Massana. 2008. Protistan assemblages across the Indian Ocean, with a specific emphasis on the picoeukaryotes. *Deep-Sea Res. Pt. I*. **55**: 1456-1473, doi:10.1016/j.dsr.2008.06.007

- Orr, J. C., V. J. Fabry, O. Aumont, L. Bopp, S. C. Doney, R. A. Feely, A. Gnanadesikan, N. Gruber, A. Ishida, F. Joos, R. M. Key, K. Lindsay, E. Maier-Reimer, R. Matear, P. Monfray, A. Mouchet, R. G. Najjar, G. K. Plattner, K. B. Rodgers, C. L. Sabine, J. L. Sarmiento, R. Schlitzer, R. D. Slater, I. J. Totterdell, M. F. Weirig, Y. Yamanaka and A. Yool. 2005. Anthropogenic ocean acidification over the twenty-first century and its impact on calcifying organisms. *Nature*. **437**: 681-686, doi:10.1038/nature04095
- Putt, M. and D. K. Stoecker. 1989. An experimentally determined carbon : volume ratio for marine oligotrichous ciliates from estuarine and coastal waters. *Limnol. Oceanogr.* **34**: 1097-1103.
- Richardson, T. L. and G. A. Jackson. 2007. Small phytoplankton and carbon export from the surface ocean. *Science*. **315**: 838-840, doi:10.1126/science.1133471
- Sabine, C. L., R. A. Feely, N. Gruber, R. M. Key, K. Lee, J. L. Bullister, R. Wanninkhof, C. S. Wong, D. W. R. Wallace, B. Tilbrook, F. J. Millero, T. H. Peng, A. Kozyr, T. Ono and A. F. Rios. 2004. The oceanic sink for anthropogenic CO₂. *Science*. **305**: 367-371.
- Sohrin, R., M. Imazawa, H. Fukuda and Y. Suzuki. 2010. Full-depth profiles of prokaryotes, heterotrophic nanoflagellates, and ciliates along a transect from the equatorial to the subarctic central Pacific Ocean. *Deep-Sea Res. Pt. II*. **57**: 1537-1550, doi:10.1016/j.dsr2.2010.02.020
- Steinberg, D. K., C. A. Carlson, N. R. Bates, R. J. Johnson, A. F. Michaels and A. H. Knap. 2001. Overview of the US JGOFS Bermuda Atlantic Time-series Study (BATS): A decade-scale look at ocean biology and biogeochemistry. *Deep-Sea Res. Pt. II*. **48**: 1405-1447.
- Strathmann, R. R. 1967. Estimating organic carbon content of phytoplankton from cell volume or plasma volume. *Limnol. Oceanogr.* **12**: 411-418.
- Strom, S. L. 2008. Microbial ecology of ocean biogeochemistry: A community perspective. *Science*. **320**: 1043-1045, doi:10.1126/science.1153527
- Venrick, E. L. 1978. The implications of subsampling, p. 75-87. *In* A. Sournia [ed.], *Phytoplankton Manual*. Unesco.
- Verity, P. G., C. Y. Robertson, C. R. Tronzo, M. G. Andrews, J. R. Nelson and M. E. Sieracki. 1992. Relationships between cell volume and the carbon and nitrogen content of marine photosynthetic nanoplankton. *Limnol. Oceanogr.* **37**: 1434-1446.

APPENDIX A
ABBREVIATIONS AND ACRONYMS USED

ASU: Arizona State University

BATS: Bermuda Atlantic Time-series Study

BIOS: Bermuda Institute of Ocean Sciences

BV: Biovolume

C: Carbon

Chl *a*: Chlorophyll *a*

CI: Confidence interval

CTD: Conductivity-temperature-depth

DAPI: 4',6-diamidino-2-phenylindole

DCM: Deep chlorophyll maximum

ENSO: El Niño-Southern Oscillation

FCM: Flow cytometry

HDF: Heterotrophic dinoflagellates

HNF: Heterotrophic nanoflagellates

HPLC: High-performance liquid chromatography

MDF: Mixotrophic dinoflagellates

MLD: Mixed layer depth

NAO: North Atlantic Oscillation

NASTG: North Atlantic Subtropical Gyre

ODV: Ocean Data View

PFA: Paraformaldehyde

R/V: Research Vessel

UV: Ultraviolet light

APPENDIX B
CRUISE DATES AND DEPTHS

Cruise ID	Approximate sampling date	Depth (m) and notes
B235 CTD2	5/29/2008	10, 40, 80, 100
B235 CTD11	5/30/2008	10, 40, 80, 100 (for 10 m, rudimentary size classes; slide too bleached to recount)
B236	6/23/2008	60, 90, 110, 120 (no 10 m slides collected for June, July, or August 2008 due to a miscommunication)
B237	7/19/2008	40, 60, 75, 100
B238	8/15/2008	60, 70, 85, 100 (15 mL filter was counted for 85 m slide)
B239	9/13/2008	10, 20, 60, 110
B240	10/8/2008	10, 20, 60, 90
B241	11/11/2008	10, 40, 80, 100
B242	12/16/2008	10, 20, 60, 120
B243 CTD2	2/8/2009	10, 40, 100, 130
B243 CTD8	2/11/2009	10, 40, 100, 130
B243a	2/23/2009	10, 60, 100, 130
B244	3/18/2009	10, 25, 60, 90
B245	4/16/2009	10, 60, 100, 110 (10 m somewhat bleached; <i>Synechococcus</i> and 1-2 μm prymnesiophytes may be underestimates)
B246	5/17/2009	10, 20, 30, 138 (10, 20, and 30 m slides somewhat bleached)
B247	6/12/2009	10, 40, 85, 100 (10 m slide uncountable due to bleaching; 40 m slide somewhat bleached)
B248	7/16/2009	10, 60, 100, 120
B249	8/16/2009	10, 25, 60, 85 (10 m slide uncountable due to bleaching)
B250	9/13/2009	10, 40, 90, 140
B251	10/10/2009	10, 60, 110, 140
B252	11/9/2009	10, 40, 90, 120
B253	12/10/2009	10, 40, 80, 120
B254	2/6/2010	10, 20, 120, 180
B255	2/25/2010	10, 40, 80, 120 (50 mL filter missing on 40 and 120 m slides; two stripes counted on 15 mL filter)
B255a	3/10/2010	10, 60, 100, 150
B256	3/26/2010	10, 40, 80, 120
B257	04/23/2010	10, 40, 80, 120